Pitch & Roll Dynamics Modeling for Vertical Orientation Control System Design

Research and Development Report

Prepared for NARCON 2026

Rev 1.1

Feb 25, 2026

Thomas B Fetter

NAR 15551

C Division

Summary

This paper is the second in a series of papers that will document the author's vertical orientation control project. The vertical orientation control rocket configuration consists of four forward mounted control canards and four rear mounted fins. The canards are rotated to control the pitch, yaw, and roll of the rocket. To design the pitch and roll control systems, a mathematical model and block diagrams of the pitch and roll rotational dynamics are needed.

Starting with the complete set of nonlinear differential equations that model the rocket's position, orientation, and frame of reference axis translation, the subset of those equations needed to model the pitch, yaw, and roll dynamics are linearized about a fixed velocity and mapped into a state space frequency domain block diagram representation. The roll model uses the differential equation that describes the rocket's rotation about its longitudinal axis resulting in a second order transfer function between the control canard angle and the rocket's roll angle. Due to a cross coupling between the two equations, the pitch model uses both the differential equation of rotation and the differential equation of lateral motion, resulting in a third order transfer function between the control canard angle and the rocket's pitch angle. The pitch block diagram also models the dynamic response to a change in the lateral wind velocity which is the main perturbing force acting on the rocket's orientation that the pitch control system must counter. The frequency domain and time domain dynamics of these rotational systems are examined in detail.

Flight data from the test rocket with the roll, pitch, and yaw control system designed using the models presented in this paper is shown to match the flight simulation very closely.

Table of Contents

1 Introduction 5
1.1 Objective and Approach 5
1.2 Prior Work 6
1.3 Acknowledgements 7
2 3-D Flight Trajectory & Rotational Dynamics Equations 8
2.1 Frames of Reference and the Coordinate Systems 8
2.2 Translating Between Axis Systems 9
2.3 State Space Model 11
2.4 Complete 3-D Flight Model 11
3 Vertical Orientation Rocket Configuration and Control Models 14
4 Roll Dynamics 17
4.1 Roll Model 17
4.2 Block Diagram for the Roll Due to the Angle of the Canards 18
4.3 Roll Dynamics 20
5 Pitch/Yaw Dynamics 24
5.1 Pitch/Yaw Model 24
5.2 Pitch Block Diagram Model 30
5.3 Block Diagram for the Pitch Rotation Due to the Wind 33
5.4 Wind Pitch Dynamics 36
5.5 Block Diagram for the Pitch Rotation Due to the Angle of the Canards 40
5.6 Canard Angle Pitch Dynamics 43
5.7 Pitch Rate vs Roll Rate Gain due to Canard Angle Rotation 46
6 Simulation vs. Flight Data Results 50
7 Conclusions, and Next Steps 53
7.1 Conclusions 53
7.2 Next Steps 53
8 Appendix 1 – Model Parameter Summary 54
9 Appendix 2 - VTS-1 Test Rocket 55
10 Appendix 3 – State Space Block Diagram of a Differential Equation 56
11 Appendix 4 – Pitch Block Diagram Transfer Function Simplification 60
12 Appendix 5 - Tools, Equipment, Facilities, & Budget 64
13 Key Variables 66
14 References 69

1 Introduction

1.1 Objective and Approach

The objective of this paper is to provide the pitch, yaw, and roll dynamics mathematical models and block diagrams that are needed to design the control system for a vertical orientation control rocket where the fins or canards are rotated to control the yaw, pitch, and roll of the rocket.

The approach is to start with the complete set of nonlinear differential equations needed to model the rocket's position, orientation, and frame of reference axis translation. Then the subset of those equations needed to model the pitch/yaw and roll dynamics are linearized about a fixed velocity and mapped into a frequency domain state space block diagram representation. The linearized state space block diagrams can then be used for the pitch, yaw, and roll control loop design, which will be covered in a future paper.

This paper is one of a series of papers that will document the author's vertical orientation control project. Figure 1-1 shows the various design tasks needed to design a rocket with a vertical orientation control system, including the modeling and design implementation tasks. This paper covers just the second box in red, Pitch and Roll Dynamics Modeling. The first paper, *Aerodynamic Parameters for Control Fins*[1], presented the aerodynamic parameters used by the dynamics models presented in this paper. Future papers will cover the other modeling tasks, including the control system design, the servo motor modeling, the vertical orientation control system rocket flight simulator, as well as the implementation of the vertical orientation control system rocket.

The nomenclature used in this paper most closely aligns with Mandell's[2] since this project started as a study of rotational dynamic stability, the topic of Mandell's chapter in *Topics in Advanced Model Rocketry*. It is consistent with the nomenclature that is used throughout the documentation of the vertical orientation control project.

A vertical orientation control system can use steerable fins or canards to control the pitch, yaw, and roll of the rocket. Canards are just a second set of fins, usually smaller than the main fins, that are used for control. For model and high power rockets, the control canards are typically located toward the front of the rocket to provide room for the servo motors. That is the rocket configuration that will be covered in detail in this paper.

---

[1] (Fetter T. B., Aerodynamic Parameters for Control Fins - vNARCON 2026 R&D Report, 2026)

[2] (Mandell, Caporaso, & Bengen, 1973)

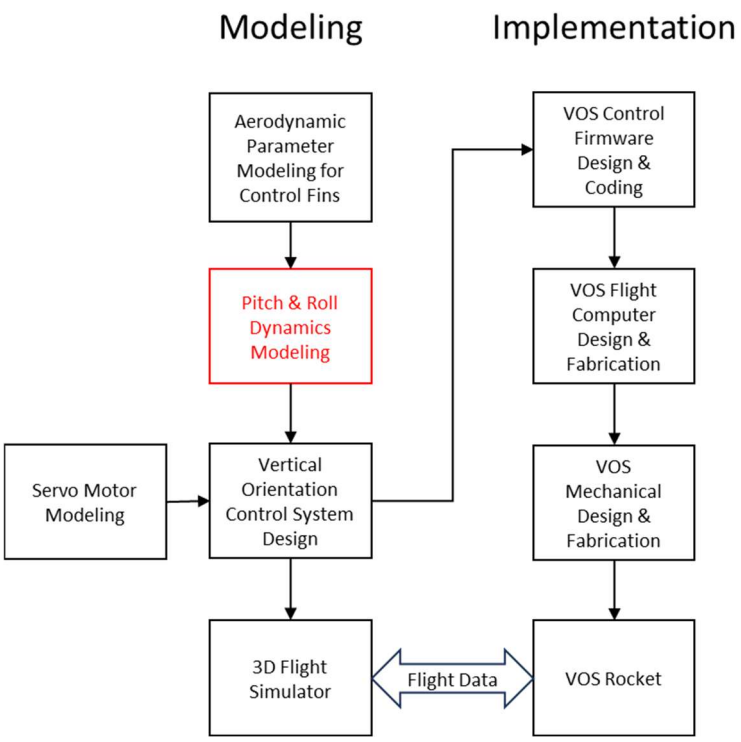

Figure 1-1 Vertical Orientation Control project

1.2 Prior Work

In *A Unified Approach to Aerodynamic Stability*, a chapter from the book *Topics in Advanced Model Rocketry*[3], Mandell describes the dynamics of a rocket's rotation about its center of gravity in free flight using Euler's dynamic equations of motion. From this, the linearized second order differential equations describing the pitch rotational dynamics of the rocket are developed, and the rotational stability is analyzed. Mandell mentions that there are side-to-side motions of the rocket that result from the angular rotation of the rocket, and that these side-to-side motions reduce the effective angle-of-attack, but he does not analyze this effect to determine its quantitative impact on the rotational dynamics.

In his NARCON 2023 R&D report, *Rotational Dynamic Stability*[4], the author showed that there is a coupling between the longitudinal (pitch and yaw) rotation equation and the lateral equation of motion that significantly impacts the rotational dynamics and stability of the rotational system. The rotational equation is combined with the

[3] (Mandell, Caporaso, & Bengen, 1973).

[4] (Fetter T. B., Rotational Dynamic Stability - vNARCON 2024 R&D Report, 2024)

lateral motion equation to produce a single coupled second order differential equation. The coupled damping ratio that comes from the combined equation shows that the rotational system is much more stable than the rotational equation alone predicts due to the side-to-side motion of the rocket. This has a direct bearing on the pitch/yaw rotation model derived in this paper.

In his NARAM 41 paper, *A Design Procedure for Maximizing Altitude Performance*[5], LaBudde presents a 3 degree of freedom model with coupling between the rotation and the X-axis motion. From that model, LaBudde derives equations for the natural frequency and damping ratio that are the same as the coupled natural frequency and damping ratio presented in the author's *Rotational Dynamic Stability* paper. The focus of LaBudde's paper is altitude optimization and he does not take the dynamic stability investigation any further into the motions of the rocket that lead to enhanced rotational stability, nor does he develop a model for the response to angled fins or canards.

The rotational dynamics models in this paper use the forcing and damping moment coefficients and equations that were presented in the author's *Aerodynamic Parameters for Control Fins*[6] R&D report.

1.3 Acknowledgements

I would like to thank Jim Jarvis for all the information he has shared about his vertical orientation control flights. A year after starting my vertical orientation project at the beginning of 2022, I saw Jim's presentation at vNARCON 2023 on his vertical orientation system. I connected with Jim shortly afterward and started doing some of the control system modeling for his flights. The flight data I have gotten from Jim over the past 3 years has been a big help in completing and validating this modeling work.

[5] (LaBudde, 1999)

[6] (Fetter T. B., Aerodynamic Parameters for Control Fins - vNARCON 2026 R&D Report, 2026)

2 3-D Flight Trajectory & Rotational Dynamics Equations

2.1 Frames of Reference and the Coordinate Systems

A complete 3-D fight model describes both the position of the center of gravity of the rocket using three position parameters and the angular orientation of the rocket using three rotational parameters, 6 degrees of freedom in total. There are two frames of reference in this model, the inertial or ground based frame of reference that remains fixed from a ground observer's point of view, and the rocket's frame of reference, which describes the movement of the rocket from the perspective of an observer on the rocket. The rocket frame of reference moves with respect to the ground frame of reference; it follows the rocket about its x and y-axes but may or may not follow the spin about the z-axis depending upon the application of the axis system.

The ground-based frame of reference axes are denoted by capital X, Y, and Z, as shown in Figure 2-1. The rocket frame of reference axes are denoted by small x, y, and z.

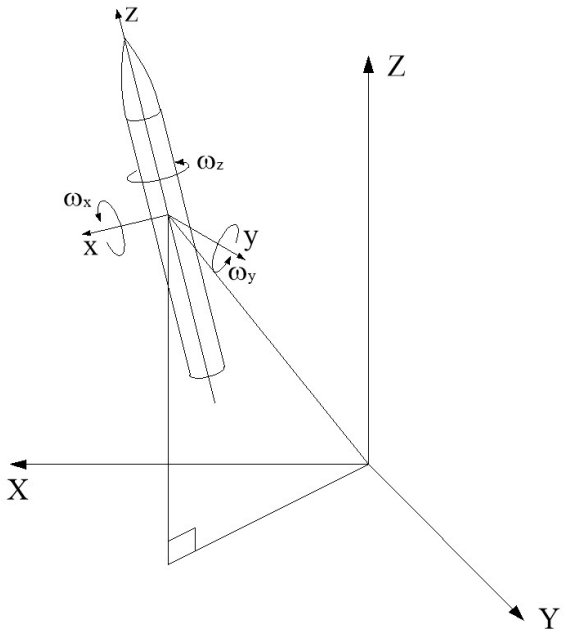

Figure 2-1 Six degrees of freedom in 3-D space

The ground frame of reference is used to describe the position of the rocket in 3-D space. For a ground observer, the orientation of the rocket will be seen in the ground frame of reference. The rocket frame of reference is needed

because the rocket's thrust, drag, and the physics of the rotation of the rocket apply to the rocket in the rocket's frame of reference. The model must then provide the means to translate between the two frames of reference.

2.2 Translating Between Axis Systems

In a 2-D system, the rocket can only rotate only about a single axis. A rotation through a single angle is all that is required to map the rocket axes into the ground frame axis system. In the 3-D system, the mapping from the x-y-z rocket frame of reference to the X-Y-Z ground frame of reference is not as simple. The rocket can rotate about all three of its axes in the rocket frame of reference, and since the x-y-z axis system follows the rocket, the x-y-z axes can be in any orientation in the ground X-Y-Z coordinate system. There are several methods for translating between coordinate systems. Euler's angles is the method used here. Quaternions and the cosine matrix are other common methods.

Euler's angles use three separate rotations to map between two 3-dimensional coordinate systems at arbitrary orientations relative to each other. Each rotation is described by an angle, so it takes three rotation angles to describe the orientation of one axis system relative to the other. The rotation angles are called the Euler's angles and are denoted ψ, θ, and ϕ. The equations that are used to map between two coordinate systems are called Euler's angle equations.

For the three Euler's angles needed to translate between the x-y-z frame rocket of reference and the X-Y-Z ground frame of reference, the order sequence in which those angles are applied, x-y-z, y-x-z, or z-x-y, etc., will affect the final orientation of the x-y-x axes in the X-Y-Z frame. For Euler's angles to work, the same rotational order used to derive the Euler's angles equations must then be used to translate between the two axis systems using those angles. A different rotation order results in a different set of Euler's angles and equations

Three sets of three equations are needed when using Euler's angles. The first two sets of equations are used to translate a coordinate point between two rotated coordinate systems using Euler's angles, one set for going each direction between the two coordinate systems. The third set of equations is used to find Euler's rotation angles for the current orientation of the two axes systems knowing the past history of the axis system rotation. The order convention means that all three sets of equations must have been derived using the same order of rotation.

There are numerous sources that cover the derivation of Euler's angles[7] that offer good explanations of the derivation. The equations used here are based upon the order of rotation conventions used in *Spacecraft Dynamics & Control*[8] in the order of rotation ϕ about x, θ about y, and ψ about z.

Euler's equations translate the coordinates of a point in one axis system into the coordinates of that point in the second axis system, where the two axis systems can be at any spatial orientation relative to each other, as described by Euler's angles. This first set of Euler's angle equations map a point, (x, y, z) in the rocket frame, into a point (X, Y, Z) in the ground frame.

$$X = (\cos\theta \cdot \cos\psi) \cdot x + (\cos\psi \cdot \sin\theta \cdot \sin\phi - \cos\phi \cdot \sin\psi) \cdot y + (\sin\psi \cdot \sin\phi + \cos\psi \cdot \cos\phi \cdot \sin\theta) \cdot z \quad (2.2\text{-}1)$$

$$Y = (\cos\theta \cdot \sin\psi) \cdot x + (\sin\theta \cdot \sin\psi \cdot \sin\phi + \cos\psi \cdot \cos\phi) \cdot y + (\cos\phi \cdot \sin\theta \cdot \sin\psi - \cos\psi \cdot \sin\phi) \cdot z \quad (2.2\text{-}2)$$

$$Z = (-\sin\theta) \cdot x + (\cos\theta \cdot \sin\phi) \cdot y + (\cos\theta \cdot \cos\phi) \cdot z \quad (2.2\text{-}3)$$

Conversely, a point in the ground frame can be mapped to the rocket frame by the second set of Euler's angle equations.

$$x = (\cos\theta \cdot \cos\psi) \cdot X + (\cos\theta \cdot \sin\psi) \cdot Y - (\sin\theta) \cdot Z \quad (2.2\text{-}4)$$

$$y = (\cos\psi \cdot \sin\theta \cdot \sin\phi - \cos\phi \cdot \sin\psi) \cdot X + (\sin\theta \cdot \sin\psi \cdot \sin\phi + \cos\psi \cdot \cos\phi) \cdot Y + (\cos\theta \cdot \sin\phi) \cdot Z \quad (2.2\text{-}5)$$

$$z = (\sin\psi \cdot \sin\phi + \cos\psi \cdot \cos\phi \cdot \sin\theta) \cdot X + (\cos\phi \cdot \sin\theta \cdot \sin\psi - \cos\psi \cdot \sin\phi) \cdot Y + (\cos\theta \cdot \cos\phi) \cdot Z \quad (2.2\text{-}6)$$

The equations above require knowing Euler's angles at any moment in time. As the rocket rotates about its axes, the rocket axes follow it, so the rocket axes rotate in the ground-based frame of reference, and the Euler's angles are changing continually. Euler's angles are calculated for any instant in time from their value at the previous instant in time and the instantaneous rotation rate about the rocket's axes. The equations that implement this are the differential form of Euler's angle equations[9]. They determine the change in Euler's angles in terms of the instantaneous rate of rotation about each of the rocket's x, y, and z-axes, ω_x, ω_y, and ω_z. Based on the same order convention used above, the differential version of Euler's equations are

$$\frac{d\phi}{dt} = \omega_x + \frac{\sin\theta \sin\phi}{\cos\theta} \cdot \omega_y + \frac{\cos\phi \sin\theta}{\cos\theta} \cdot \omega_z \quad (2.2\text{-}7)$$

---

[7] Two examples are (Thomson, 1986, p. Chapter 3) and (Sidi, 2002, p. Appendix A)

[8] (Sidi, 2002, p. 321)

[9] These rotation rate equations are consistent with the conventions used above, but the derivation is shown in (Thomson, 1986, p. 38) using a different order of rotation convention

$$\frac{d\theta}{dt} = \cos\phi \cdot \omega_y - \sin\phi \cdot \omega_z \tag{2.2-8}$$

$$\frac{d\psi}{dt} = \frac{\sin\phi}{\cos\theta} \cdot \omega_y + \frac{\cos\phi}{\cos\theta} \cdot \omega_z \tag{2.2-9}$$

Solving these three differential equations using the rocket frame of reference rotation rates as the inputs provides Euler's angles for any point in time which can then be used to translate any point between the two frames of reference using Euler's angle equations above. In addition to the rocket's orientation, quantities, such as distance, velocity, and acceleration, can all be translated between the frames of reference using Euler's angles.

In the rocket, the sensor that is used to determine the rate of rotation about the rocket's three axes, and hence the rocket's orientation, is a rate gyroscope. A rate gyroscope provides the rate of rotation, ω, about each of the rocket's three axes, *x*, *y*, and *z*, from which Euler's angles are calculated.

2.3 State Space Model

For the 3-D flight model, all the differential equations will be written in state space form. In state space form, all differential equations are written as first order differential equations, where an n^{th} order differential equation can be written as *n* first order differential equations. The resulting first order differential variables are the state variables of the system.

The state variables of a system of differential equations are the minimum set of variables needed to describe the complete state of the system at any point in time. All other parameters needed to describe the system can then be determined from algebraic functions in terms of the state variables.

The state space form of the block diagram, with all first order integrator blocks (see Appendix 3), makes it easier to analyze the system because it exposes all the key state variable parameters that describe the system. A state space diagram is also needed for the design of the vertical orientation controller if a state space type of controller is being used.

2.4 Complete 3-D Flight Model

The location of the center of gravity of the rocket in 3-D space is determined in the ground based frame of reference using Newton's law, $F = m \cdot a$. There are six independent equations, (2.4-1) - (2.4-6) , when written in state space form, needed to determine the location and velocity along each of the three orthogonal axes. The forces acting on the rocket along the X, Y, and Z-axes are the X, Y, and Z components of the thrust, drag, and lift forces, as well as the force due to gravity along the Z-axis. Some of these forces are determined in the rocket frame of reference and then translated to the ground frame of reference.

$$m_o \frac{d}{dt} v_X = F_{TX} + F_{DX} + F_{LX} \tag{2.4-1}$$

$$\frac{d}{dt} d_X = v_X \tag{2.4-2}$$

$$m_o \frac{d}{dt} v_Y = F_{TY} + F_{DY} + F_{LY} \tag{2.4-3}$$

$$\frac{d}{dt} d_Y = v_Y \tag{2.4-4}$$

$$m_o \frac{d}{dt} v_Z = F_{TZ} + F_{DZ} + F_{LZ} - m_o g \tag{2.4-5}$$

$$\frac{d}{dt} d_Z = v_Z \tag{2.4-6}$$

The physics of the rotation of the rocket apply to the rocket in the rocket's frame of reference. The rotation of the rocket about its center of gravity is determined in the rocket frame of reference using Euler's dynamic equations[10] (different than Euler's angle equations). Eulers's dynamic equations are the rotational version of Newton's law. There is both a forcing[11] moment and a damping moment that act on the rocket along each of its three axes Two of the rotational equations include a coupling term that is proportional to the product of the difference in the moment of inertia and rotation rate about the other two axes. There is no cross-coupling term for the z-axis equation due to the symmetry of the x and y-axes for a rocket ($I_{Lx} = I_{Ly} \Rightarrow I_{Lx} - I_{Ly} = 0$).

$$I_L \frac{d\omega_x}{dt} = M_{2x} + M_{1x} + (I_L - I_R) \cdot \omega_y \cdot \omega_z \tag{2.4-7}$$

$$\frac{d}{dt} \alpha_x = \omega_x \tag{2.4-8}$$

---

[10] (Mandell, Caporaso, & Bengen, 1973, p. 78)

[11] Barrowman uses "forcing moment" and Mandell uses "corrective moment" for the zero order term in the rotational equations. This paper uses the forcing moment nomenclature.

$$I_L \frac{d\omega_y}{dt} = M_{2y} + M_{1y} + (I_R - I_L) \cdot \omega_x \cdot \omega_z \tag{2.4-9}$$

$$\frac{d}{dt}\alpha_y = \omega_y \tag{2.4-10}$$

$$I_R \frac{d\omega_z}{dt} = M_{2z} + M_{1z} \tag{2.4-11}$$

$$\frac{d}{dt}\alpha_z = \omega_z \tag{2.4-12}$$

The translation from the inertial (ground) frame of reference and the rocket frame of reference is provided by the differential version of Euler's angle equations that determine Euler's angles from the rate of rotation about each of the rocket's three axes as described in Section 2.2.

$$\frac{d\phi}{dt} = \omega_x + \frac{\sin\theta \sin\phi}{\cos\theta} \cdot \omega_y + \frac{\cos\phi \sin\theta}{\cos\theta} \cdot \omega_z \tag{2.4-13}$$

$$\frac{d\theta}{dt} = \cos\phi \cdot \omega_y - \sin\phi \cdot \omega_z \tag{2.4-14}$$

$$\frac{d\psi}{dt} = \frac{\sin\phi}{\cos\theta} \cdot \omega_y + \frac{\cos\phi}{\cos\theta} \cdot \omega_z \tag{2.4-15}$$

The 15 state variables for the system of 15 equations (2.4-1) - (2.4-15), determined from the differential values on the left side of each equation, are $d_X, d_Y, d_Z, v_X, v_Y, v_Z, \alpha_x, \alpha_y, \alpha_z, \omega_x, \omega_y, \omega_z, \phi, \theta, \psi$.

Parameters that are determined in one of the frames of reference but used in the other frame of reference use the Euler's angles to make the translation. For example, since the thrust, drag, and lift forces are determined in the rocket frame of reference but used on the ground frame of reference for the position equations (2.4-1)-(2.4-5), the X, Y, and Z components of these forces are calculated from the x, y, and z components using Euler's angles and Euler's Equations (2.2-1) -(2.2-3).

3 Vertical Orientation Rocket Configuration and Control Models

Figure 3-1 shows a typical configuration for a rocket with control canards along with the canard rotations used for roll and pitch control. Three separate control systems are used, one for pitch, one for yaw, and one for roll. Four control canards are used. To control pitch, the two y-axis canards are moved as a pair in the same direction on the y-axis. To control yaw, the two x-axis canards are moved as a pair in the same direction on the x-axis. For roll control, all four canards rotate together; with opposite canards rotated in opposite directions on their respective axes. For calculating the pitch and yaw normal force, only two canards and fins are used for each, but for roll, all four fins and canards are used. Because the pitch and yaw control systems are orthogonal, they are independent for small pitch and yaw rotations.

The graphs in this paper showing the typical values for various dynamic parameters are based on the vertical orientation system test rocket VTS-1. The key dimensions for VTS-1 are given in Appendix 2. As explained in the author's R&D paper, *Aerodynamic Parameters from Control Fins*[12] , VTS-1 uses a free rotating tail section, or spin can, so that the forward mounted canards are effective for roll control. The spin-can eliminates the downwash interference because fins that are free to roll or spin cannot generate a counter torque on the rocket. Pitch and yaw control are not affected by the spin can or by the downwash from the canards.

To model the flight of a rocket with a vertical orientation control system, the complete 3-D model from Section 2, along with the control system equations, is used. But to design the roll, pitch, and yaw control loops, a different model is needed. Because control systems are most easily designed in the frequency domain and involve pole/zero placement to shape the system response, a frequency domain model is needed. The frequency domain model is created by taking the Laplace transform of a linearized version of the time domain model differential equations[13].

The frequency domain model is a linearized model that describes the dynamics of the roll or pitch rotations in response to a change in the canard angles. The full 3-D model rotational equations are nonlinear, in part, because they are functions of the velocity of the rocket. The coefficients in the linearized equations are still a function of the velocity of the rocket, but when the velocity is held at a fixed value, the equations can be linear. The control loop can then be evaluated over a range of velocities to evaluate the response and stability of the control loop at each velocity. The equations are also nonlinear because they include trigonometric functions of the rotation angles. These are linearized by assuming the rotation angles are small.

---

[12] (Fetter T. B., Aerodynamic Parameters for Control Fins - vNARCON 2026 R&D Report, 2026)

[13] See the paper (Fetter T. B., Linear Systems and Control Systems Overview, 2024) for an overview of the linear systems mathematical concepts for differential equations, the Laplace transform, the frequency domain, and the poles and zeros of the system equation

Since pitch and yaw are symmetrical for a typical rocket, only one model is needed to describe both. A second model is needed for the roll dynamics. Because the roll and pitch dynamics models come from a subset of the equations in the complete 3-D flight model described in Section 2.3, they each have a smaller number of degrees of freedom than the full 6 degrees of freedom of the 3-D model.

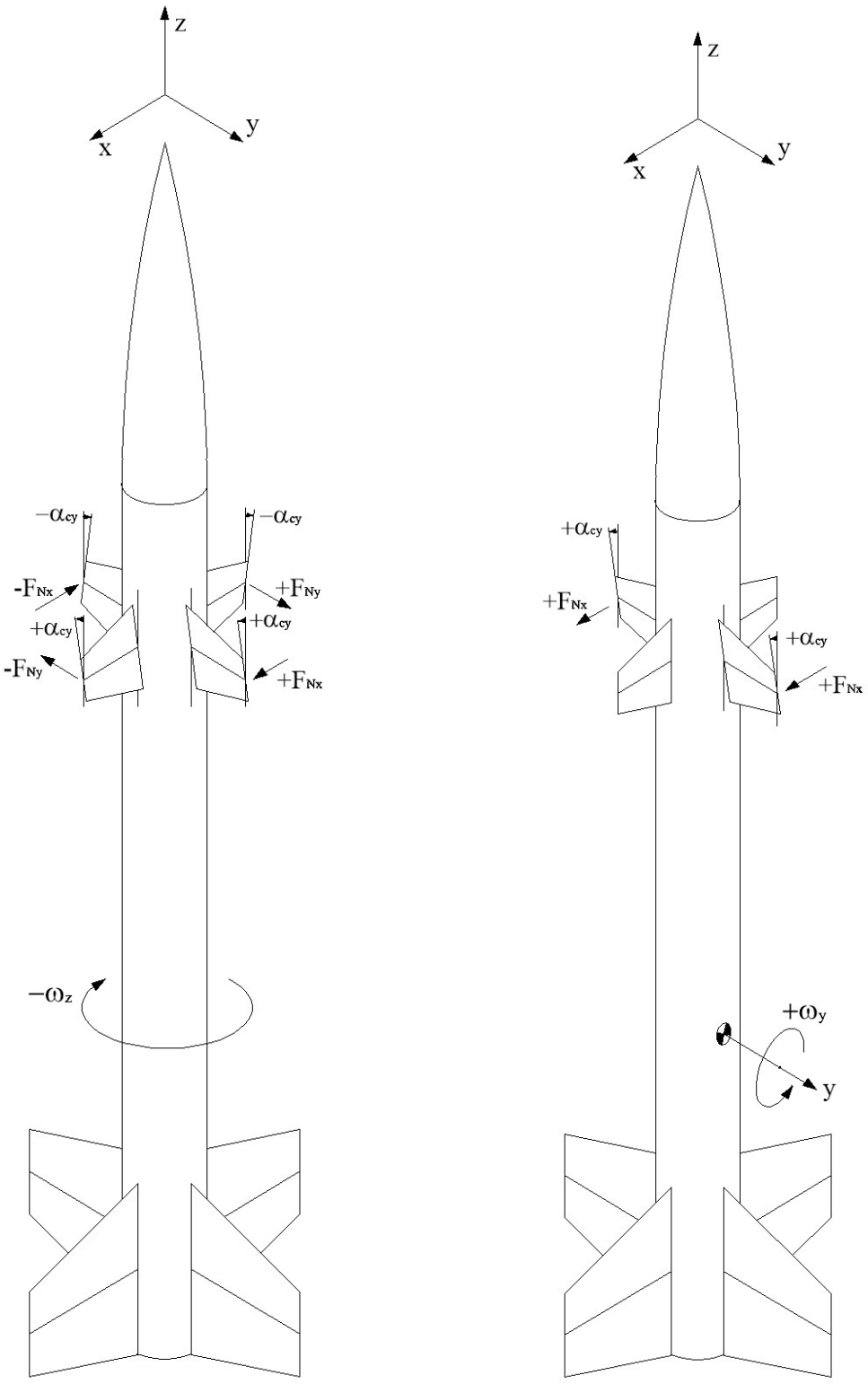

Figure 3-1 Typical vertical orientation control rocket configuration showing roll and pitch control

4 Roll Dynamics

4.1 Roll Model

The roll model describes how the rocket rolls in response to a change in the angle of the canards. The roll model comes from the z-axis rotation equations (2.4-11) and (2.4-12), which are

$$I_R \frac{d\omega_z}{dt} = M_{2z} + M_{1z} \tag{4.1-1}$$

$$\frac{d}{dt}\alpha_z = \omega_z \tag{4.1-2}$$

For the rocket configuration shown in Figure 3-1, only the canards will contribute to the roll forcing moment. And if a spin-can is being used, then only the canards will contribute to the roll damping moment as well. If a spin can is not being used, which might be the case of the canards are mounted behind the fins, then both the canards and fins will contribute to the roll damping moment.

From Appendix 1 of *Aerodynamic Parameters from Control Fins*[14], the roll forcing moment,

$$M_{1z} = -\frac{\rho}{2} \cdot A_r \cdot {v_{Tz}}^2 \cdot CA_{Rc} \cdot C_{N\alpha Rc} \cdot k_{TBc} \cdot \alpha_c \tag{4.1-3}$$

and the roll damping moment, assuming a spin can is being used, is

$$M_{2z} = -\frac{\rho}{2} \cdot A_r \cdot \left|v_{Tz}\right| \cdot {CM_{Rc}}^2 \cdot C_{N\alpha Rc} \cdot \omega_z \tag{4.1-4}$$

The fin normal force coefficient, $C_{N\alpha R}$, the fin radial center of area, CA_R, the radius of gyration, CM_R, and the tail/body interference factor due to fin rotation, k_{TB}, are all defined in the *Aerodynamic Parameters from Control Fins* paper. The z-axis component of the total oncoming airstream velocity, v_{Tz}, will be treated as a constant. It is only the z-axis component of the total airstream vector that causes the roll of the rocket. The z-axis component of the total airstream velocity has a sign, but to be consistent with the total airstream velocity use for pitch, the magnitude of v_{Tz} is used in the roll damping moment, and the sign of the moment is then set to ensure it has the correct rotational direction.

---

[14] (Fetter T. B., Aerodynamic Parameters for Control Fins - vNARCON 2026 R&D Report, 2026)

The input variable, α_c and state variable, ω_z, are separated out of the moments by defining coefficients comprised of the remaining terms

$$C_{1z} = -\frac{\rho}{2} \cdot A_r \cdot {v_{Tz}}^2 \cdot CA_{Rc} \cdot C_{N\alpha Rc} \tag{4.1-5}$$

and

$$C_{2z} = \frac{\rho}{2} \cdot A_r \cdot \left|v_{Tz}\right| \cdot {CM_{Rc}}^2 \cdot C_{N\alpha Rc} \tag{4.1-6}$$

If a spin can is not being used, which might be the case if the canards are mounted behind the fins, then both the canards and fins will contribute to the damping moment. If the fins are fixed, the roll damping moment coefficient is

$$C_{2z} = \frac{\rho}{2} \cdot A_r \cdot \left|v_{Tz}\right| \cdot \left({CM_{Rc}}^2 \cdot C_{N\alpha Rc} + {CM_{Rf}}^2 \cdot C_{N\alpha Rf} \right) \tag{4.1-7}$$

Using the roll coefficients, equation (4.1-1), in terms of the input variable and state variable, becomes

$$I_R \frac{d\omega_z}{dt} + C_{2z} \cdot \omega_z = C_{1z} \cdot \alpha_c \tag{4.1-8}$$

where the terms have been rearranged so that the input term, α_c, is on the right side of the equals sign, and the state variable response terms are on the left side. The coefficients C_{1z} and C_{2z} are both functions of velocity, and therefore also functions of time. But at a fixed velocity, C_{1z} and C_{2z} are fixed, and the equation is a linear, first order differential equation. This differential equation says that, in the long term, the roll rate is proportional to the angle of the canard, determined by the zero order term, but with transitional dynamics due to the first order term.

4.2 Block Diagram for the Roll Due to the Angle of the Canards

Taking the Laplace transform[15] of equation (4.1-8) and rearranging the terms, the frequency domain transfer function for roll rate is

$$G_s = \frac{\omega_z}{\alpha_c} = \frac{C_{1z}}{I_R} \cdot \frac{1}{s + \frac{C_{2z}}{I_R}} \tag{4.2-1}$$

[15] See (Fetter T. B., Linear Systems and Control Systems Overview, 2024)

where the complex frequency $s = j \cdot \omega$.

The roll gain equation (4.2-1) is a first order frequency domain differential equation. Using the state space block diagram representation for a first order equation (see Appendix 3), the transfer function for the roll gain, equation (4.2-1), can be mapped by inspection onto the block diagram shown in Figure 4-1. The gain block at the input accounts for the C_{1z}/I_R term of the equation.

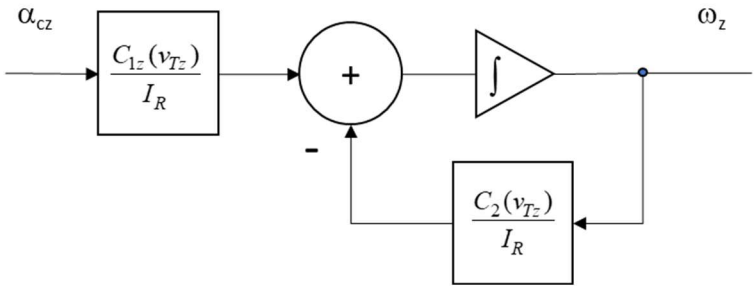

Figure 4-1 Roll rate block diagram of equation (4.2-1)

The roll control system will control the roll angle, not just the roll rate, so the roll dynamics block diagram needs to include the roll angle as the output. To go from the roll rate of Figure 4-1 to the roll angle, an integrator is added, since the roll angle is the integral of the roll rate. Figure 4-2 shows the complete block diagram for equations (4.1-1) and (4.1-2).

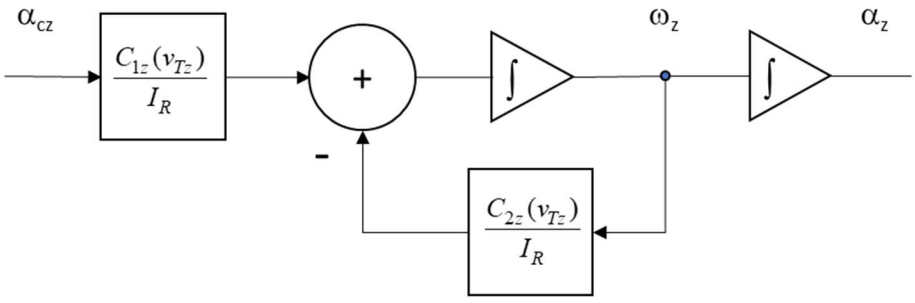

Figure 4-2 Complete roll block diagram with roll rate and roll angle

The transfer function for the roll angle is the second order equation

$$\frac{\alpha_z}{\alpha_c} = \frac{C_{1z}}{I_R} \cdot \frac{1}{s \cdot \left(s + \frac{C_{2z}}{I_R} \right)} \tag{4.2-2}$$

4.3 Roll Dynamics

Figure 4-3 shows a Bode plot[16] of the magnitude of the frequency domain roll rate gain from equation (4.2-1) for various airstream velocities for the vertical orientation test rocket VTS-1. This plot shows the magnitude of the roll rate response to a sinusoidal change in the canard angle at the frequency of the x-axis of the plot. It shows that this is a low pass system with a single pole roll-off. The gain of the roll rate is flat up to the corner frequency, or bandwidth of the system. The gain in this region, the steady state gain, is the ratio of the forcing moment coefficient to the damping moment coefficient,

$$K_s = \frac{C_{1z}}{C_{2z}} \tag{4.3-1}$$

and the corner frequency is given by

$$\omega_{ns} = \frac{C_{2z}}{I_R} \tag{4.3-2}$$

which is proportional to the damping coefficient and inversely proportional to the radial moment of inertia.

Below the corner frequency, the change in roll rate keeps up with the rate of the change in the canard angle. Above the corner frequency, the change in roll rate starts to fall off as the rotation rate of the canards increases. Both the gain and the bandwidth are functions of the airstream velocity, the higher the velocity, the larger the gain and the wider the bandwidth. The rocket rolls faster at a given canard angle and responds to faster changes in the canard angle at higher airstream velocities.

Because the rotation rate gain is flat below the natural frequency, this says that that a fixed non-zero canard angle produces a fixed roll rotation rate, and that the roll angle from equation (4.2-2) would be a liner ramp since it is the integral of the roll rate.

[16] (Fetter T. B., Linear Systems and Control Systems Overview, 2024)

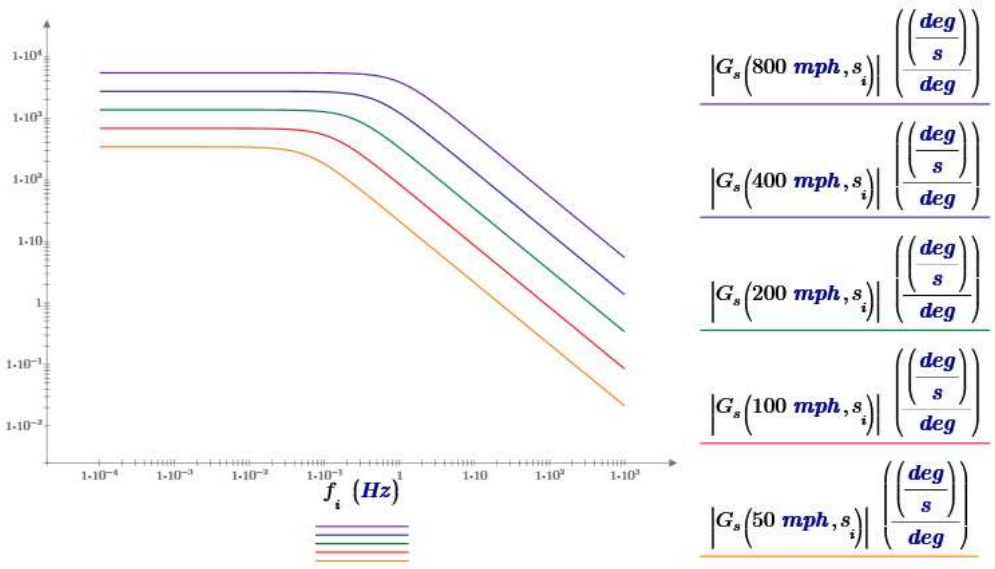

Figure 4-3 Frequency response of the roll rate gain function

Figure 4-4 is a plot of the steady state roll rate gain per degree rotation of the canards for VTS-1 from equation (4.2-1) in units of (deg/sec)/deg. The roll rate increases linearly with velocity. The roll rate also increases linearly with the canard rotation angle, so, for a 2 deg rotation angle, the roll rate would be twice the value shown in the graph. VTS-1 uses a spin can, so the rotation rate is high because the main fins are not providing any damping. With fixed fins, the rotation rate would be lower. At 200 mph, 1 deg of canard rotation produces 4 roll rotations per second, so the roll rate is very sensitive to the canard rotation angle.

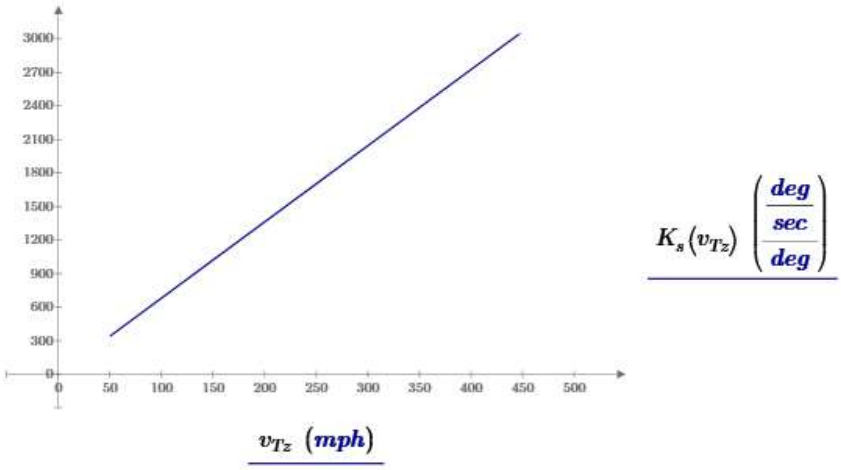

Figure 4-4 Steady state gain vs. airstream velocity

Figure 4-5 is a plot of the corner frequency, or bandwidth of the system, as a function of the airstream velocity from equation (4.3-2). It shows that the bandwidth also increases linearly with the airstream velocity.

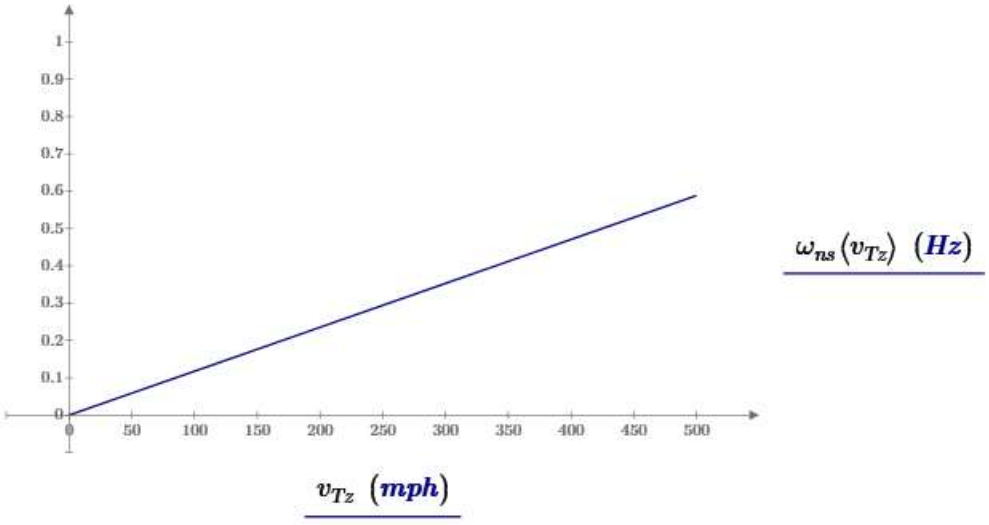

Figure 4-5 Bandwidth vs airstream velocity

To characterize the system in the time domain, a step response is used[17]. In this case, the angle of the canards is stepped, and the roll rate response is determined. The Laplace transform of a unit step is $1/s$, so the time domain step response is the inverse Laplace transform of equation (4.2-1) times α_c/s, where α_c is the size of the step of the canard angle

$$\begin{aligned}\omega_{z\,step} &= \mathcal{L}^{-1}\left(\frac{\omega_z}{\alpha_c}\cdot\frac{\alpha_c}{s}\right) = \mathcal{L}^{-1}\left(\left(\frac{C_{1z}}{C_{2z}}\cdot\frac{1}{\frac{I_R}{C_{2z}}\cdot s+1}\right)\cdot\frac{\alpha_c}{s}\right)\\ &= -\alpha_c\cdot\frac{C_{1z}}{C_{2z}}\cdot\left(e^{\frac{-(C_{2z}\cdot t)}{I_R}}-1\right) = \alpha_c\cdot K_s\cdot\left(e^{\frac{-(C_{2z}\cdot t)}{I_R}}-1\right)\end{aligned} \tag{4.3-3}$$

[17] (Fetter T. B., Linear Systems and Control Systems Overview, 2024, pp. 12-14)

Figure 4-6 shows a plot of the roll rate response to a 1 degree step in the canard angle for various airstream velocities. The final value for the step response is the steady state gain, K_s times the size of the input step of the canard angle, in this case, 1 degree. A 2 degree step would produce twice the roll rate shown in the graph. The rise time is inversely proportional to the corner frequency, ω_{ns}. The higher the airstream velocity, the larger the steady state spin rate, and the faster the time to the steady state level. The flat final response shows that, after the initial transient response, the rocket rolls at a constant rate for a given angle rotation of the canards.

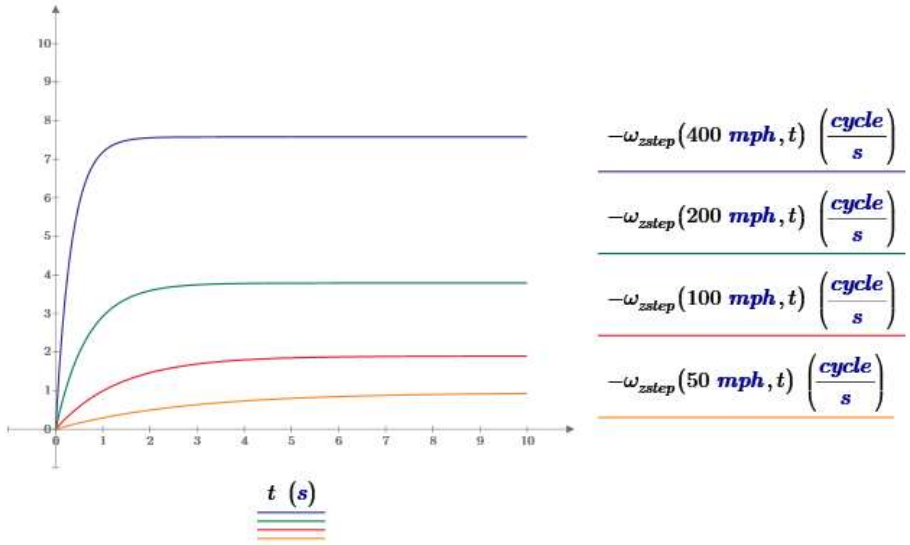

Figure 4-6 Roll rate **s**tep response for a 1 deg step in the canard angle for various airstream velocities

5 Pitch/Yaw Dynamics

5.1 Pitch/Yaw Model

The pitch and yaw model describes how the rocket rotates in pitch or yaw in response to a change in the angle of the canards. Since the pitch and yaw are controlled by two orthogonal and independent control loops, each acting on a single axis of rotation of the rocket, the complete 3-D model of Section 2.3 can be simplified to a 2-D model. The pitch and yaw models are essentially the same; the pitch notation will be used to develop the model. Pitch is the rotation about the rocket's y-axis, so the pitch model comes from the y-axis rotation equations (2.4-9) and (2.4-10)

$$I_L \frac{d\omega_y}{dt} = M_{2y} + M_{1y} + (I_R - I_L)\cdot\omega_x\cdot\omega_z \tag{5.1-1}$$

$$\frac{d}{dt}\alpha_y = \omega_y \tag{5.1-2}$$

From Appendix 1 of *Aerodynamic Parameters from Control Fins*[18] the form of the pitch forcing moment is

$$M_{1y} = \frac{\rho}{2}\cdot A_r\cdot {v_T}^2\cdot\left(L_{CP} - L_{CG}\right)\cdot C_{N\alpha}\cdot\alpha_{at} \tag{5.1-3}$$

All the parameters except for the angle-of-attack and airstream velocity are constants determined by the geometry of the rocket. The airstream velocity will be treated as a constant. The angle-of-attack is a variable quantity that is not an input to the system, or a state variable, so it must be found in terms of inputs and state variables. Figure 5-1 shows that the angle-of-attack, α_{at}, is the difference between the direction of the total incoming airstream, α_T, and the rotation angle of the rocket, α_y

$$\alpha_{at} = \alpha_T - \alpha_y \tag{5.1-4}$$

and that the angle of the oncoming airstream, α_T, is

$$\alpha_T = \arcsin\left(\frac{v_X - v_w}{v_T}\right) \simeq \frac{v_X - v_w}{v_T} \tag{5.1-5}$$

so the angle-of-attack is

[18] (Fetter T. B., Aerodynamic Parameters for Control Fins - vNARCON 2026 R&D Report, 2026)

$$\alpha_{at} = \frac{v_X}{v_T} - \frac{v_w}{v_T} - \alpha_y \tag{5.1-6}$$

where v_w, the wind velocity, is an input to the system, v_T, the total oncoming airstream velocity, will be treated as a constant, and α_y and v_X are state variables of the 3-D system. α_y comes from the y-axis rotational equation (5.1-1), but v_X is an input to the rotational equation that comes from the X-axis equation of motion (2.4-1). This says that there is a cross coupling between the y-axis rotational equation and the X-axis equation of motion, so both equations must be included in the pitch rotation model. In fact, the y-axis rotational angle of the rocket is an input to the X-axis equation of motion because the X-axis equation of motion also includes the angle-of-attack of the rocket in the lift force. Both equations are cross coupled with each other.

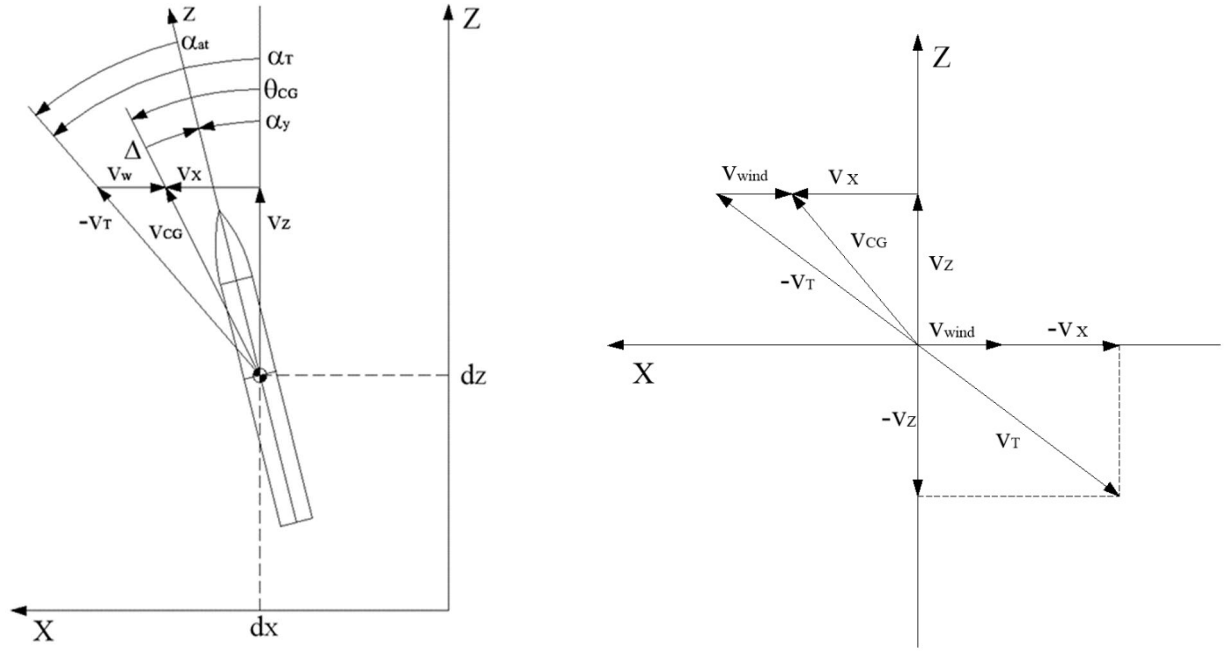

Figure 5-1 Key two dimensional rotation angles

The paper *Rotational Dynamic Stability*[19] showed the cross coupling between the X-axis equation of motion and the y-axis rotational equation is through the X-axis lift force term. The X-axis thrust and drag forces are shown to contribute little to the coupling, so they can be eliminated from the X-axis equation of motion in this model. Like

[19] (Fetter T. B., Rotational Dynamic Stability - vNARCON 2024 R&D Report, 2024)

the roll model, the linearized pitch model will apply about a single airstream velocity, so the equation of motion that describes the change in velocity of the rocket along the Z-axis can also be eliminated. It is also assumed that the roll rate is zero (since the orientation control system will set the roll rate to zero), so the x-axis cross coupling term shown in equation (5.1-1) goes to zero. The remaining equations and parameters from the model 3-D model needed for the pitch rotation model are

$$m_o \frac{dv_X}{dt} = F_{LX} \tag{5.1-7}$$

$$I_L \frac{d\omega_y}{dt} = M_2 + M_1 \tag{5.1-8}$$

$$\frac{d}{dt}\alpha_y = \omega_y \tag{5.1-9}$$

Now the pitch rotation model consisting of the differential equations (5.1-7) to (5.1-9) can be developed in terms of the aerodynamic parameters for the rocket components.

For the rocket configuration shown in Figure 3-1, the nosecone, fins, and canards all contribute to the pitch forcing and damping moments. At small angles of attack, the body tube has a negligible impact on the pitch moments, which is why Barrowman does not include it in his stability calculations. The spin-can does not affect the pitch rotation, so it does not matter if one is being used.

From Appendix 1 of *Aerodynamic Parameters from Control Fins*[20] and TIR-33[21], the pitch forcing moment is comprised of the moments due to the nosecone, fins, and canards

$$M_{1ync} = \frac{\rho}{2} \cdot A_r \cdot {v_T}^2 \cdot \left(L_{CPnc} - L_{CG}\right) \cdot C_{N\alpha nc} \cdot \alpha_{at} \tag{5.1-10}$$

$$M_{1yf} = \frac{\rho}{2} \cdot A_r \cdot {v_T}^2 \cdot \left(L_{CPf} - L_{CG}\right) \cdot C_{N\alpha Tf} \cdot K_{TBf} \cdot \alpha_{at} \tag{5.1-11}$$

$$M_{1yc} = \frac{\rho}{2} \cdot A_r \cdot {v_T}^2 \cdot \left(L_{CPc} - L_{CG}\right) \cdot C_{N\alpha Tc} \cdot \left(K_{TBc} \cdot \alpha_{at} + k_{TBc} \cdot \alpha_c\right) \tag{5.1-12}$$

If the portion of the forcing moment due to the rotation angle of the canard is separated out, and the remaining term due to the body angle-of-attack is summed with the fin and nosecone moments, the result is the total moment that would be seen by the rocket due only to its angle-of-attack. With this regrouping, the two pitch forcing moments acting on the rocket are

---

[20] (Fetter T. B., Aerodynamic Parameters for Control Fins - vNARCON 2026 R&D Report, 2026)

[21] (Barrowman, 1968)

$$M_{1y} = \frac{\rho}{2} A_r \cdot {v_T}^2 \cdot \left(L_{CP} - L_{CG}\right) \cdot C_{N\alpha TB} \cdot \alpha_{at} \tag{5.1-13}$$

$$M_{1yc} = \frac{\rho}{2} A_r \cdot {v_T}^2 \cdot \left(L_{CPc} - L_{CG}\right) \cdot C_{N\alpha Tc} \cdot k_{TBc} \cdot \alpha_c \tag{5.1-14}$$

where the total normal force coefficient for the rocket including the tail/body interference factors that multiply the body angle-of-attack is

$$C_{N\alpha TB} = C_{N\alpha nc} + C_{N\alpha Tf} \cdot K_{TBf} + C_{N\alpha Tc} \cdot K_{TBc} \tag{5.1-15}$$

The rocket's center of pressure, which includes the tail/body interference factors, is

$$L_{CP} = \frac{C_{N\alpha nc} \cdot L_{CPnc} + C_{N\alpha Tf} \cdot K_{TBf} \cdot L_{CPf} + C_{N\alpha Tc} \cdot K_{TBc} \cdot L_{CPc}}{C_{N\alpha nc} + C_{N\alpha Tf} \cdot K_{TBf} + C_{N\alpha Tc} \cdot K_{TBc}} \tag{5.1-16}$$

From Appendix 1 of *Aerodynamic Parameters from Control Fins and Canards*, the canard damping moment has no separate portion due to the rotation angle of the canards. The total damping moment due to the nosecone, fins, and canards can be treated just like the total rocket forcing moment from equation (5.1-13) where the induced angle-of-attack is due to the tangential rotational velocity at the rocket's center of pressure.

$$M_{2y} = -\frac{\rho}{2} \cdot A_r \cdot \left|v_T\right| \cdot \left(L_{CP} - L_{CG}\right)^2 \cdot C_{N\alpha} \cdot \omega_y \tag{5.1-17}$$

where the total normal force coefficient without the tail/body interference factor is used for the damping moment

$$C_{N\alpha} = C_{N\alpha nc} + C_{N\alpha Tf} + C_{N\alpha Tc} \tag{5.1-18}$$

v_T is the positive magnitude of the total oncoming airstream vector. The sign of the damping moment is set assuming the airstream velocity is a positive quantity so that it has the correct rotational direction.

The canard angle input variable, α_c, the body angle-of-attack, α_{at}, and the pitch rotation rate state variable, ω_y, are separated out of the moments in equations (5.1-13), (5.1-14), and (5.1-17) by defining coefficients comprised of the remaining terms

$$C_1 = \frac{\rho}{2} \cdot A_r \cdot {v_T}^2 \cdot \left(L_{CP} - L_{CG}\right) \cdot C_{N\alpha TB} \tag{5.1-19}$$

$$C_{1c} = \frac{\rho}{2} \cdot A_r \cdot {v_T}^2 \cdot \left(L_{CPc} - L_{CG}\right) \cdot C_{N\alpha Tc} \tag{5.1-20}$$

$$C_2 = \frac{\rho}{2} \cdot A_r \cdot \left|v_T\right| \cdot \left(L_{CP} - L_{CG}\right)^2 \cdot C_{N\alpha} \tag{5.1-21}$$

Then, equation (5.1-8) can be written as

$$I_L \frac{d^2\alpha_y}{dt^2} = -C_2 \cdot \frac{d\alpha_y}{dt} + C_1 \cdot \alpha_{at} - C_{1c} \cdot \alpha_c \tag{5.1-22}$$

Figure 5-1 shows that the angle-of-attack, α_{at}, is the difference between the direction of the total incoming airstream, α_T, and the rotation angle of the rocket, α_y

$$\alpha_{at} = \alpha_T - \alpha_y \tag{5.1-23}$$

Substituting this into equation (5.1-22) and arranging the state variable on the left side of the equals sign

$$I_L \cdot \frac{d^2}{dt^2}\alpha_y + C_2 \cdot \frac{d}{dt}\alpha_y + C_1 \cdot \alpha_y = C_1 \cdot \alpha_T - C_{1c} \cdot \alpha_c \tag{5.1-24}$$

The two inputs to the rocket's rotation are the angle of the oncoming airstream and the rotation angle of the canards. Equation (5.1-24) says that, when the canard angle is 0 deg, the rocket rotates until it is aligned with the oncoming airstream.

From Figure 5-1, the angle of the oncoming airstream, α_T, is

$$\alpha_T = \arcsin\left(\frac{v_X - v_w}{v_T}\right) \simeq \frac{v_X - v_w}{v_T} \tag{5.1-25}$$

and substituting this into equation (5.1-24) gives

$$I_L \cdot \frac{d^2}{dt^2}\alpha_y + C_2 \cdot \frac{d}{dt}\alpha_y + C_1 \cdot \alpha_y = -C_1 \cdot \frac{v_w}{v_T} + C_1 \cdot \frac{v_X}{v_T} - C_{1c} \cdot \alpha_c \tag{5.1-26}$$

Again, v_T is the positive magnitude of the total airstream vector. Figure 5-1 shows a vector labeled $-v_T$, but this is just to indicate that it is a vector pointing in the opposite direction of the actual airstream vector, v_T.

The three inputs to the pitch rotation equation (5.1-26) are the velocity of the wind, v_w, the rotation angle of the canards, α_c, and the ground frame of reference X-axis velocity, v_X. It is the v_X input term to the y-axis rotation equation that causes the coupling with the X-axis equation of motion.

For the X-axis equation of motion (5.1-7), the lift force is given by

$$F_L = \frac{\rho}{2} \cdot A_r \cdot v_T^{\,2} \cdot \left(C_{L\alpha TB} \cdot \alpha_{at} - C_{L\alpha Tc} \cdot \alpha_c \right) \tag{5.1-27}$$

and from Figure 5-2, the ground frame X-axis lift force is

$$F_{LX} = -F_L \cdot \cos\left(\alpha_T\right) \simeq -\frac{\rho}{2} \cdot A_r \cdot v_T^{\,2} \cdot \left(C_{L\alpha TB} \cdot \alpha_{at} - C_{L\alpha Tc} \cdot \alpha_c \right) \tag{5.1-28}$$

for small α_T.

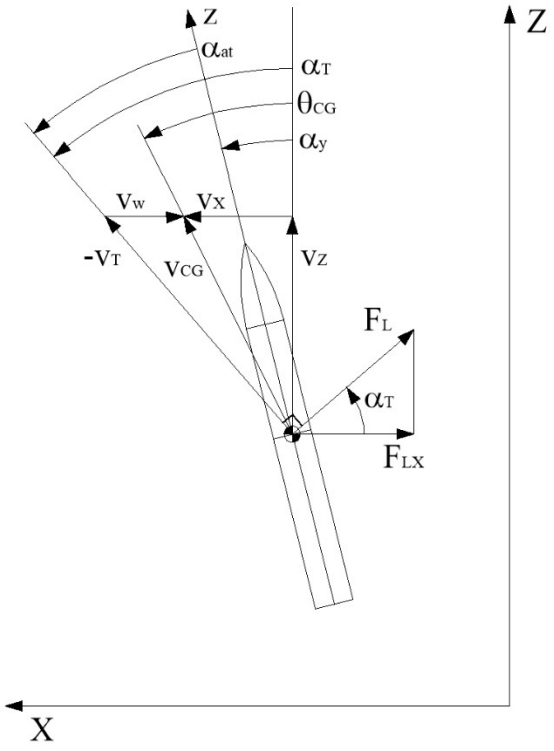

Figure 5-2 Calculation of the lift force

Separating out the angle-of-attack and the canard rotation angles in equation (5.1-28) by defining the lift coefficients

$$C_3 = \frac{\rho}{2} \cdot A_r \cdot C_{L\alpha TB} \cdot {v_T}^2 \tag{5.1-29}$$

$$C_{3c} = \frac{\rho}{2} \cdot A_r \cdot C_{L\alpha Tc} \cdot {v_T}^2 \tag{5.1-30}$$

At small angles of attack

$$C_{L\alpha TB} \simeq C_{N\alpha TB} \tag{5.1-31}$$

$$C_{L\alpha Tc} \simeq C_{N\alpha Tc} \tag{5.1-32}$$

Then, equation (5.1-7) can be written as

$$m_o \frac{dv_X}{dt} = -C_3 \cdot \alpha_{at} + C_{3c} \cdot \alpha_c \tag{5.1-33}$$

Using equations (5.1-23) and (5.1-25) to replace α_{at} and rearranging the terms with the state variable on the left and the inputs on the right side of the equation

$$m_o \frac{d}{dt} v_X + C_3 \cdot \frac{v_X}{v_T} = C_{3\cdot} \cdot \frac{v_w}{v_T} + C_3 \cdot \alpha_y + C_{3c} \cdot \alpha_c \tag{5.1-34}$$

The three inputs to the X-axis equation of motion (5.1-34) are the velocity of the wind, v_w, the rotation angle of the canards, α_c, and the rocket frame of reference y-axis rocket rotation angle, α_y. It is the α_y input term to the X-axis equation of motion causes the coupling with the y-axis equation of rotation.

5.2 Pitch Block Diagram Model

Taking the Laplace transform of the pitch rotation equation (5.1-26) and rearranging the terms

$$\alpha_y = \left(-\frac{C_1}{I_L \cdot v_T} \cdot v_w - \frac{C_{1c}}{I_L} \cdot \alpha_c + \frac{C_1}{I_L \cdot v_T} \cdot v_X \right) \cdot \frac{1}{s^2 \cdot + \frac{C_2}{I_L} \cdot s + \frac{C_1}{I_L}} \tag{5.2-1}$$

The frequency domain pitch equation (5.2-1) is a second order differential equation, so the second order state space block diagram is used (see Appendix 3). By inspection, equation (5.2-1) maps into the block diagram shown in Figure 5-3.

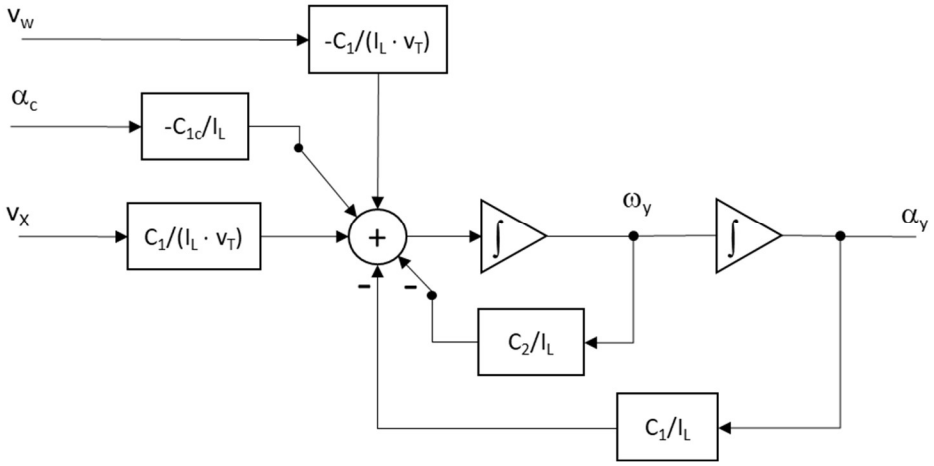

Figure 5-3 y-axis rotational equation block diagram

Taking the Laplace transform of the X-axis equation of motion (5.1-34) and rearranging the terms

$$v_X = \left(\frac{C_3}{m_o \cdot v_T} \cdot v_w + \frac{C_{3c}}{m_o} \cdot \alpha_c + \frac{C_3}{m_o} \cdot \alpha_y \right) \cdot \frac{1}{s + \frac{C_3}{m_o \cdot v_T}} \tag{5.2-2}$$

The frequency domain X-axis equation of motion (5.2-2) is a first order differential equation, so the first order state space block diagram is used (see Appendix 3). By inspection, equation (5.2-2) maps into the block diagram shown in Figure 5-4.

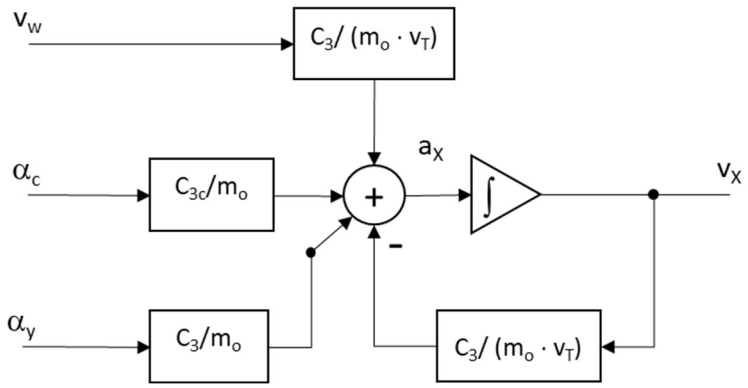

Figure 5-4 X-axis equation of motion

Each block diagram above has three inputs and one output. Two of the inputs, the wind velocity, v_w, and the canard rotation angle, α_c, are external inputs to the system. But the X-axis velocity, v_X, and the y-axis rotation angle, α_y, are state variable outputs for each system. To supply the state variables as inputs, these two block diagrams can be interconnected so that the rotation equation block diagram supplies the rotation angle to the X-axis equation of motion block diagram, and the X-axis equation of motion block diagram supplies the X-axis velocity to the rotation equation block diagram. The interconnected system block diagram is shown in Figure 5-5. It has just two external inputs, v_w and α_c, and one output, α_y, which is the state variable of interest for the vertical orientation control system design. This block diagram could just as easily be arranged so that the v_X state variable is the final output, but that is not the primary variable of interest. No matter which way the block diagram is arranged, there is no impact to the values of the state variables.

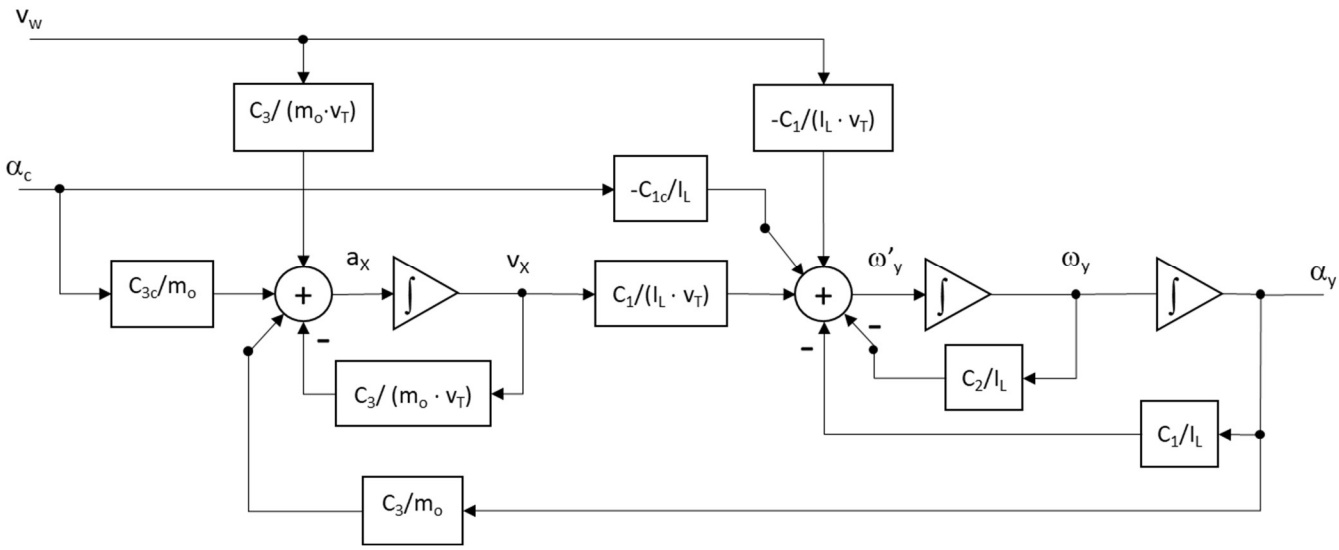

Figure 5-5 Combined pitch rotation system

Determining the transfer function for the canard angle to roll rate was straight forward because that system consists of a single differential equation with a single input. But the pitch system comes from two simultaneous differential equations with two inputs. Each input will have its own transfer function to the output angle. This is a linear system, at a fixed airstream velocity, so the output angle will be the linear sum of the component due to the wind and the component due to the canard angle. This system is a third order system as determined by the three integrators. And because it has feed forward paths, it also includes frequency dependent terms in the numerator of the transfer function, or zeros.

5.3 Block Diagram for the Pitch Rotation Due to the Wind

The wind transfer function describes the rocket's rotational angle response to a change in the lateral wind velocity. The transfer function for the wind is determined from the block diagram in Figure 5-5 by setting the canard angle input to zero and then simplifying the block diagram down to a single block. The block diagram can be simplified by one of two methods. Either sets of blocks can be combined into single blocks repeatedly until a single gain block is reached with the complete transfer equation, or the node equations for the block diagram can be written, resulting in a series of simultaneous algebraic equations that can then be combined into a single transfer equation. For simple block diagrams, combining blocks is easy, but it does not always work if there are many interleaved signal paths. The node equation method always provides a solution, and when combined with Mathcad's capability of solving a series of simultaneous algebraic equations symbolically, this method is easy even for complex block diagrams.

The node equation method was used to determine the wind velocity to rotation angle transfer function (see Appendix 4 for a compete derivation). The resulting transfer function is

$$G_w = \frac{\alpha_y}{v_w} = \frac{-C_1}{I_L \cdot v_T} \cdot \frac{1}{s^2 + \frac{C_2 \cdot m_o \cdot v_T + C_3 \cdot I_L}{I_L \cdot m_o \cdot v_T} \cdot s + \frac{C_2 \cdot C_3 + C_1 \cdot m_o \cdot v_T}{I_L \cdot m_o \cdot v_T}} \tag{5.3-1}$$

Equation (5.3-1) is a second order equation, even though the coupled system shown in Figure 5-6 that it comes from a third order system. The order reduction happens because certain terms cancel each other in the process of the block diagram reduction in a way that eliminates the highest order term for that transfer function.

Equation (5.3-1) can be mapped back onto a second order state space block diagram by inspection as shown in Figure 5-6. This is the simplified block diagram for the coupled rotational equation.

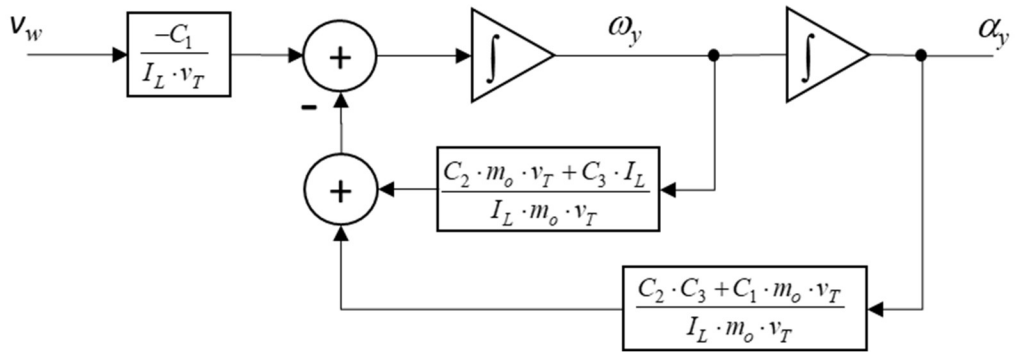

Figure 5-6 Simplified wind velocity to rotation angle block diagram

Equation (5.3-1) is called the coupled rotational equation because it is the combination of the rotational equation (5.2-1) coupled with the X-axis equation of motion (5.2-2). It is a second order differential equation, like the rotational equation, but the coefficients are different. The coupled rotational equation determines the dynamics, including the degree of stability, of the rocket's pitch rotational response to a wind perturbation. The paper, *Rotational Dynamic Stability*[22], shows that the response from the coupled rotational equation is far more stable than the response predicted by the pitch rotational equation alone.

Equation (5.3-1) can be written in the form

$$G_w = \frac{\alpha_y}{v_w} = \frac{-C_1}{v_T} \cdot \frac{1}{I_L \cdot s^2 + C_2' \cdot s + C_1'} \tag{5.3-2}$$

where C_1' and C_2' represent the coupled forcing and damping coefficients, where

$$C_1' = C_1 + \frac{C_2 \cdot C_3}{v_T \cdot m_o} \tag{5.3-3}$$

and

$$C_2' = C_2 + \frac{C_3 \cdot I_L}{v_T \cdot m_o} \tag{5.3-4}$$

[22] (Fetter T. B., Rotational Dynamic Stability - vNARCON 2024 R&D Report, 2024)

which is the form used in the *Rotational Dynamic Stability* paper[23]. Equations (5.3-3) and (5.3-4) clearly show how the rotational forcing and damping coefficients are modified by the terms that come from the coupling with the X-axis equation of motion.

There are two parameters that describe the response of a second order differential equation[24], the natural frequency, ω_n, and the damping ratio, ζ. A second order frequency domain differential equation can be written in the form

$$G(s) = G_0 \cdot \frac{1}{\frac{s^2}{\omega_n{}^2} + \frac{2 \cdot \zeta \cdot s}{\omega_n} + 1} = G_0 \cdot \frac{\omega_n{}^2}{s^2 + 2 \cdot \zeta \cdot \omega_n \cdot s + \omega_n{}^2} \tag{5.3-5}$$

Putting the rotational equation (5.3-1) into this form, the resulting natural frequency and damping ratio evaluated for test rocket VTS-1 at 200 mph are

$$\omega_n{}' = \sqrt{\frac{C_1 + \frac{C_2 \cdot C_3}{v_T \cdot m_o}}{I_L}} = 1.857 Hz \tag{5.3-6}$$

$$\zeta' = \sqrt{\frac{\left(C_2 + \frac{C_3 \cdot I_L}{v_T \cdot m_o}\right)^2}{4 \cdot \left(C_1 + \frac{C_2 \cdot C_3}{v_T \cdot m_o}\right) \cdot I_L}} = 0.067 \tag{5.3-7}$$

Doing the same for the uncoupled rotational equation (5.2-1), the resulting natural frequency and damping ratio for test rocket VTS-1 are

$$\omega_n = \sqrt{\frac{C_1}{I_L}} = 1.855 Hz \tag{5.3-8}$$

$$\zeta = \sqrt{\frac{C_2{}^2}{4 \cdot C_1 \cdot I_L}} = 0.0073 \tag{5.3-9}$$

---

[23] (Fetter T. B., Rotational Dynamic Stability - vNARCON 2024 R&D Report, 2024, pp. 31-32)

[24] (Fetter T. B., Linear Systems and Control Systems Overview, 2024, pp. 16-23)

The coupled and uncoupled natural frequency are virtually the same, but the coupled damping ration is more than 9 times the uncoupled damping ration for VTS-1. That means that the coupled system is significantly more stable than the rotational equation alone would predict.

The reason for the greater stability when the X-axis motion of the rocket is included, as explained in the *Rotational Dynamic Stability* paper, is that there is a small side-to-side motion of the rocket that creates an induced angle-of-attack like the induced angle-of-attack created by the pitch rotation. The side-to-side velocity is in phase with the tangential rotational velocity, so it adds to the magnitude of the damping term. The side-to-side velocity is significantly greater than the tangential rotational velocity at the center of pressure, so the damping due to the side-to-side velocity is significantly greater than the damping due to the tangential rotational velocity, and it is the X-axis velocity term that determines the rotational stability of the rocket.

The damping factor and the natural frequency describe the location of the poles of the rotation equation. The design for the vertical orientation control system requires an accurate model of the rotational transfer function and the corresponding location of the poles of the system. The coupled equation correctly models the rotational dynamics, whereas the rotational equation alone does not.

5.4 Wind Pitch Dynamics

The wind is a perturbing force that causes the rocket to rotate in pitch or yaw away from a vertical flight path. In most cases, this is the major perturbation for which the vertical orientation pitch control system will need to correct to keep the rocket in a vertical orientation. The design objective for the control system is to reduce the susceptibility of the rocket to the wind. The measure of the effectiveness of the control system is the difference in gains to the wind with and without the control system. So it is first important to understand the wind gain without the control loop in place.

Figure 5-7 shows a Bode plot of the magnitude of the wind velocity gain function (5.3-1) for various airstream velocities for the vertical orientation test rocket VTS-1. This plot shows how the magnitude of the pitch angle responds to a sinusoidal change in the wind velocity at the frequency of the x-axis of the plot. It shows that this is a low pass system with a two pole roll-off. The gain to the wind velocity is flat up to the natural frequency ω_n. The gain in this region, which is the steady state gain, is

$$K_w = \frac{-C_1 \cdot m_o}{C_2 \cdot C_3 + C_1 \cdot m_o \cdot v_T} \tag{5.4-1}$$

and the natural frequency, which is close to the bandwidth for a second order system, is given by equation (5.3-6). Equation (5.3-6) is the coupled natural frequency. The coupled natural frequency is close to the uncoupled natural frequency from equation (5.3-8), so the natural frequency can be simplified to

$$\omega_n' = \sqrt{\frac{C_1 + \frac{C_2 \cdot C_3}{v_T \cdot m_o}}{I_L}} \simeq \sqrt{\frac{C_1}{I_L}} \tag{5.4-2}$$

Below the natural frequency, the gain to the wind is flat, and above the natural frequency, the response to a change in the wind drops off rapidly. Because the rotation angle gain to the wind is flat below the natural frequency, this says that that a fixed non-zero wind velocity produces a fixed pitch rotation angle. Both the gain and the bandwidth are functions of the airstream velocity; the higher the velocity the less the rocket will rotate in response to the wind. But at higher velocities, the rocket will respond to faster rate changes in the wind.

The peaking in the frequency response of a second order system is determined by the damping ratio, which is given by equation (5.3-7). The magnitude of the peak is reduced significantly by the damping provided by the side-to-side X-axis motion of the rocket.

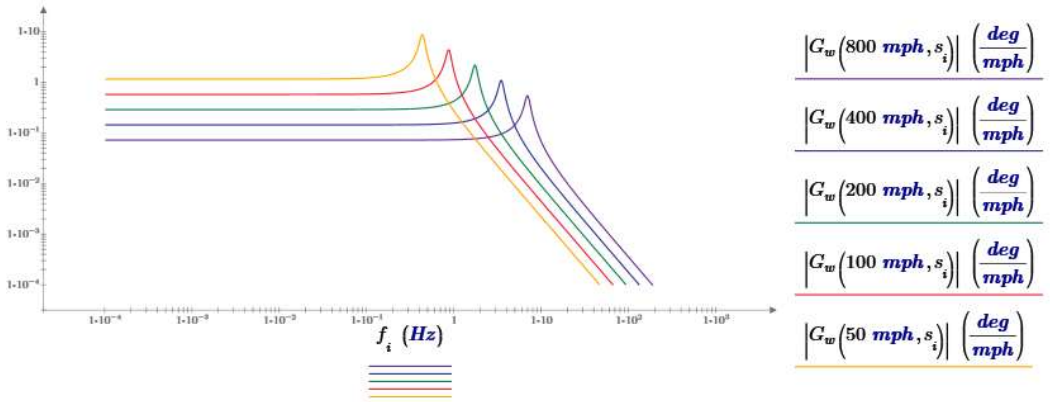

Figure 5-7 Frequency response of the wind pitch gain function in deg/mph of wind velocity

Figure 5-8 shows the steady pitch angle gain per mph of wind velocity vs. the total airstream velocity for VTS-1 from equation (5.4-1). It shows the gain decreases with increasing airstream velocity.

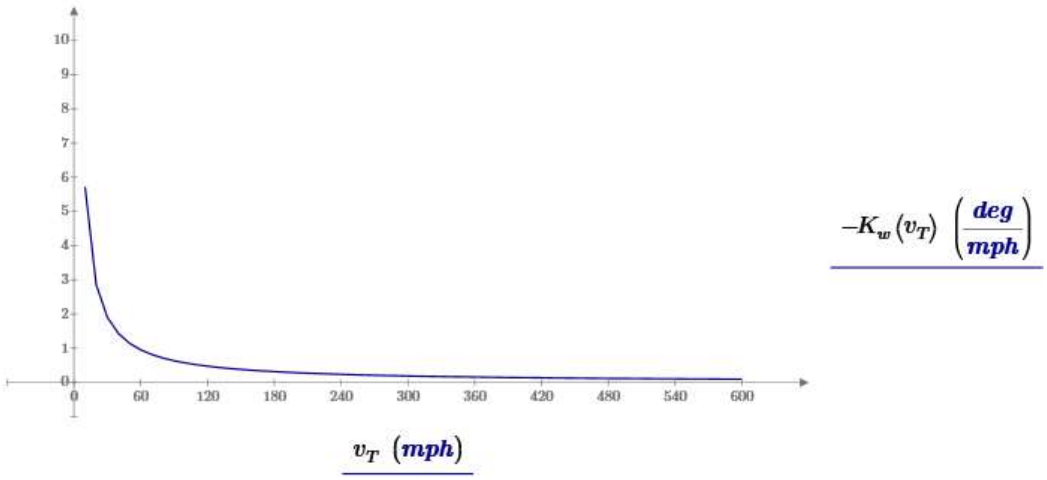

Figure 5-8 Steady state gain vs. airstream velocity

Figure 5-9 is a plot of the natural frequency of the system, from equations (5.4-2), and Figure 5-10 is a plot of the damping ratio, from equation (5.4-2), both as a functions of the airstream velocity. The natural frequency increases linearly with the velocity, but the damping ratio is nearly constant with velocity, which says that the stability of the rocket is not a function of its velocity[25].

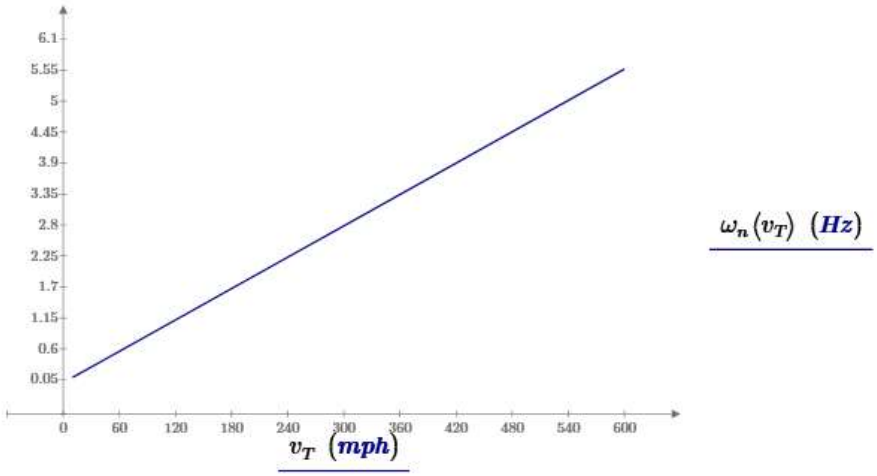

Figure 5-9 Bandwidth vs airstream velocity

[25] This does not include the effects of the change in the center of pressure with angle of attack which is a function of the rockets velocity. See (Galejs, 1999)

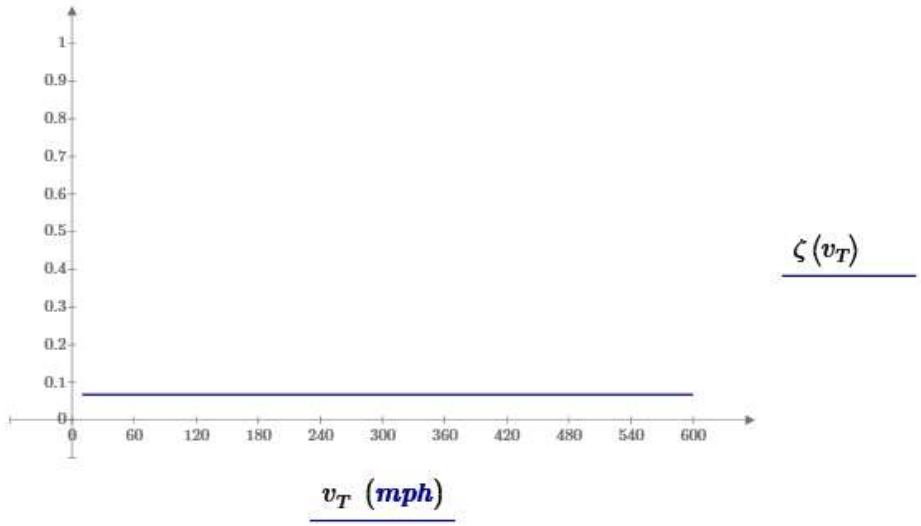

Figure 5-10 Damping ratio vs. airstream velocity

To characterize the system in the time domain, a step response is used. In this case, the velocity of the wind is stepped, and the pitch angle response is determined. The Laplace transform of a unit step is $1/s$, so the time domain step response is the inverse Laplace transform of equation (5.3-5) times v_w/s, where v_w is the size of the wind velocity step

$$\alpha_{ywindstep} = \mathcal{L}^{-1}\left(\frac{\alpha_y}{v_w}\cdot\frac{v_w}{s}\right) = \mathcal{L}^{-1}\left(\left(K_w\cdot\frac{1}{\frac{s^2}{\omega_n{}^2}+\frac{2\cdot\zeta\cdot s}{\omega_n}+1}\right)\cdot\frac{v_w}{s}\right) = \tag{5.4-3}$$
$$v_w\cdot K_w\cdot\left(\begin{array}{l}-\frac{\zeta\cdot\omega_n}{\sqrt{(-\zeta^2+1)\cdot\omega_n{}^2}}\cdot e^{-(\zeta\cdot\omega_n\cdot t)}\cdot\sin\left(t\cdot\sqrt{(-\zeta^2+1)\cdot\omega_n{}^2}\right)- \\ e^{-(\zeta\cdot\omega_n\cdot t)}\cdot\cos\left(t\cdot\sqrt{(-\zeta^2+1)\cdot\omega_n{}^2}\right)+1\end{array}\right)$$

Figure 5-11 shows a plot of the pitch angle response to a step in the wind velocity at an airstream velocity of 200 mph. The final value for the step response is the steady state gain, K_w times the size of the input step in wind velocity, in this case, 1 mph. A 2 mph step would produce twice the pitch rotation shown in the graph. The rise time is roughly proportional to $1/\omega_n$, the frequency of the ringing is ω_n, and the magnitude of the ringing envelope is a function of the damping ratio, ζ. The larger the damping ratio, the smaller the magnitude of the ringing, and

the faster it settles to its final value. The flat final response says that, after the initial transient response settles, the rocket rotates in pitch to a constant angle for a given step in the wind velocity.

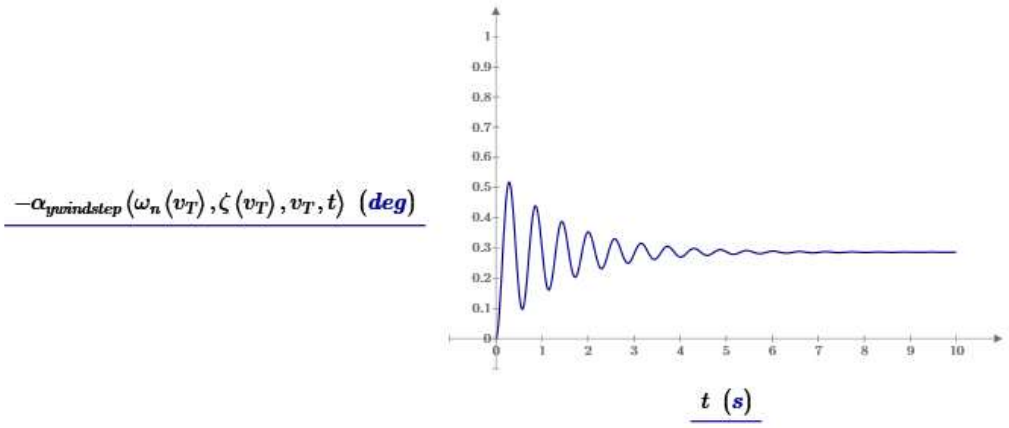

Figure 5-11 Pitch angle response to a 1 mph step in the wind velocity at a total airstream velocity of 200 mph

Because this step response is for a fixed airstream velocity, it represents the response for small incremental steps in the wind velocity. It cannot be used to determine the magnitude of the rocket's rotation as it leaves the launch guide because the rocket's velocity is changing rapidly during the time it takes to complete that rotation. To determine the size of the rotation, the complete nonlinear 2-D or 3-D flight model must be used[26]

5.5 Block Diagram for the Pitch Rotation Due to the Angle of the Canards

The canard angle transfer function describes the rocket's rotational response to a change in the rotational angle of the canards. The transfer function for the canard angle is determined from the block diagram in Figure 5-5 by setting the wind input to zero and then writing the node equations and solving them (see Appendix 4 for the complete derivation). The resulting transfer function is

$$G_c = \frac{\alpha_y}{\alpha_c} = \frac{-C_{1c}}{I_L} \cdot \frac{s + \dfrac{C_3 \cdot C_{1c} - C_1 \cdot C_{3c}}{C_{1c} \cdot m_o \cdot v_T}}{s \cdot \left(s^2 + \dfrac{C_2 \cdot m_o \cdot v_T + C_3 \cdot I_L}{I_L \cdot m_o \cdot v_T} \cdot s + \dfrac{C_2 \cdot C_3 + C_1 \cdot m_o \cdot v_T}{I_L \cdot m_o \cdot v_T} \right)} \tag{5.5-1}$$

[26] See (Fetter T. B., How Far Does a Rocket Turn Into the Wind, 2024)

Equation (5.5-1) is a third order system equation with a single zero in the numerator. Unlike the second order pitch rotation transfer function due to the wind, the canard angle transfer function retains all three poles from the combination of the second order y-axis rotation equation and the first order X-axis equation of motion. It can be mapped by inspection onto a third order state space block diagram that includes a zero (see Appendix 3) with the result shown in Figure 5-12. The trick to doing this is to first multiply the second order equation in the denominator by the $1/s$ term so that equation (5.5-1) becomes

$$G_c = \frac{\alpha_y}{\alpha_c} = \frac{-C_{1c}}{I_L} \cdot \frac{s + \dfrac{C_3 \cdot C_{1c} - C_1 \cdot C_{3c}}{C_{1c} \cdot m_o \cdot v_T}}{s^3 + \dfrac{C_2 \cdot m_o \cdot v_T + C_3 \cdot I_L}{I_L \cdot m_o \cdot v_T} \cdot s^2 + \dfrac{C_2 \cdot C_3 + C_1 \cdot m_o \cdot v_T}{I_L \cdot m_o \cdot v_T} \cdot s + 0} \tag{5.5-2}$$

With that, the zero order coefficient of that resulting equation is 0, so there is no feedback path from the third integrator.

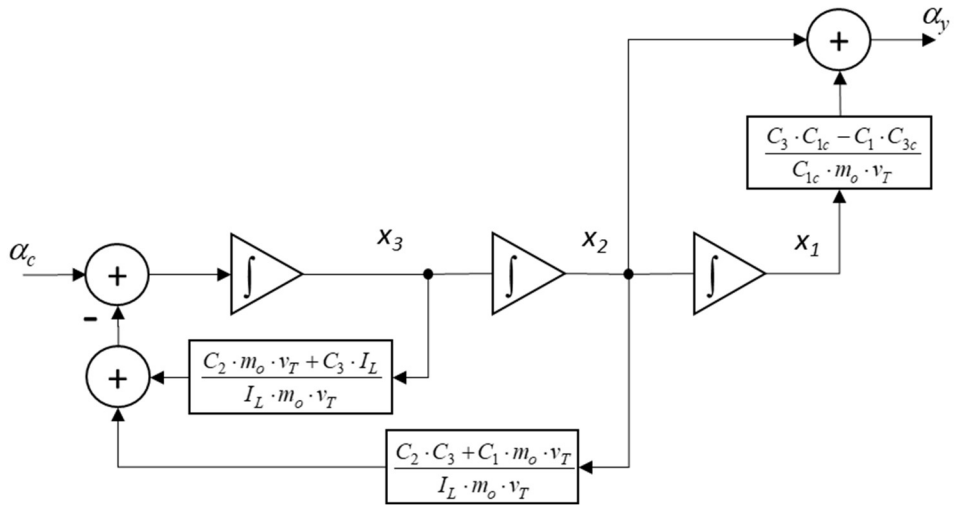

Figure 5-12 Simplified wind velocity to rotation angle block diagram

Although the block diagram in Figure 5-12 gives the correct pitch angle output for a given canard angle input, it does not expose the pitch rotation rate, the parameter measured by the gyroscope sensor, which is needed to implement the control design. The output angle is the integral of the rotation rate, so an integrator is needed right at the output of the block diagram. The block diagram in Figure 5-12 can be rearranged to provide this. The third integrator can be pulled through the final gain block and output summer if a differentiator is added to the other input of the output summer to maintain the same path gains. That differentiator can then be removed if that signal path is moved to the other side of the second integrator by moving the connection from node x_2 to node x_3. Doing that

provides the differentiation for that path. The result is shown in Figure 5-13. This same result can be obtained by starting with the transfer function for ω_y/α_c by dropping the $1/s$ term in equation (5.5-1) and then adding an integrator to the output to go from ω_y to α_y.

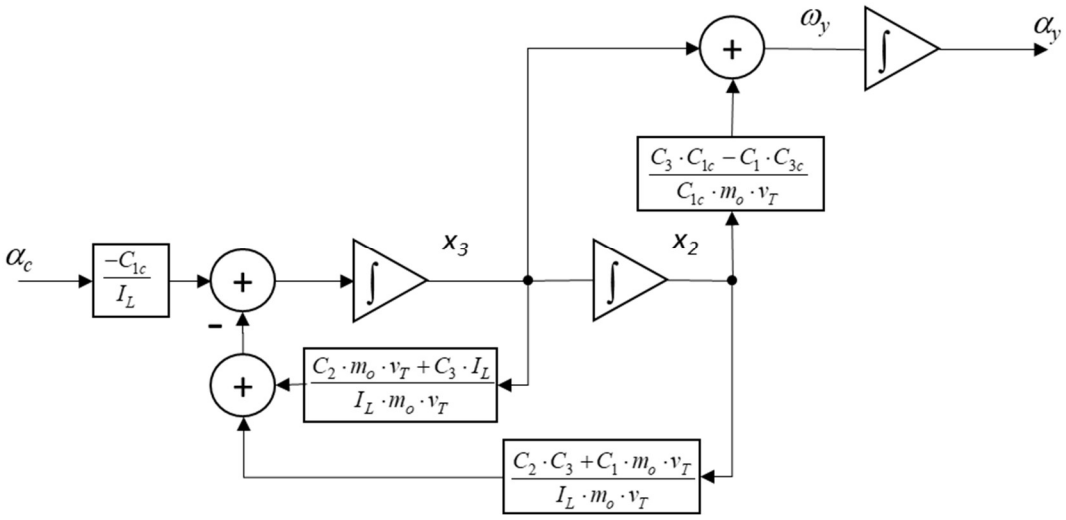

Figure 5-13 Simplified wind velocity to rotation angle block diagram modified to expose the rotation rate state variable

The transfer function from the canard angle to the pitch rotation rate is then

$$G_{c\omega} = \frac{\omega_y}{\alpha_c} = \frac{-C_{1c}}{I_L} \cdot \frac{s + \dfrac{C_3 \cdot C_{1c} - C_1 \cdot C_{3c}}{C_{1c} \cdot m_o \cdot v_T}}{\left(s^2 + \dfrac{C_2 \cdot m_o \cdot v_T + C_3 \cdot I_L}{I_L \cdot m_o \cdot v_T} \cdot s + \dfrac{C_2 \cdot C_3 + C_1 \cdot m_o \cdot v_T}{I_L \cdot m_o \cdot v_T} \right)} \tag{5.5-3}$$

And the transfer function from the canard angle to the pitch rotation angle is the integral of equation (5.5-3)

$$G_c = \frac{\alpha_y}{\alpha_c} = \frac{-C_{1c}}{I_L} \cdot \frac{s + \dfrac{C_3 \cdot C_{1c} - C_1 \cdot C_{3c}}{C_{1c} \cdot m_o \cdot v_T}}{s \cdot \left(s^2 + \dfrac{C_2 \cdot m_o \cdot v_T + C_3 \cdot I_L}{I_L \cdot m_o \cdot v_T} \cdot s + \dfrac{C_2 \cdot C_3 + C_1 \cdot m_o \cdot v_T}{I_L \cdot m_o \cdot v_T} \right)} \tag{5.5-4}$$

which is the same as equation (5.5-1). Like the wind velocity transfer function, the canard angle transfer function has parameters from both the rotation equation and the X-axis equation of motion, so the coupled system is required to properly model the rotation of the rocket due to the rotation angle of the canards.

5.6 Canard Angle Pitch Dynamics

Figure 5-14 shows the Bode plot of the magnitude of the canard angle transfer function for the pitch rotation rate, equation (5.5-4), for various airstream velocities for the vertical orientation test rocket VTS-1 in units of (degrees/s)/deg of rotation rate per degree of canard angle. It has a second order differential equation as the denominator with the same coefficients as the wind velocity transfer function, along with zero in the numerator. Because the rotation rate gain is flat below the natural frequency, this says that that a fixed non-zero canard angle produces a fixed pitch rotation rate. The gain in this region is given by

$$K_{c\omega} = \frac{C_1 \cdot C_{3c} - C_3 \cdot C_{1c}}{C_2 \cdot C_3 + C_1 \cdot m_o \cdot v_T} \tag{5.6-1}$$

The natural frequency and damping ratio of the second order portion of the equation are the same as the parameters for the rotation due to the wind equation as described by equations (5.3-6) and (5.3-7). The frequency of the zero is given by

$$\omega_o = \frac{C_3 \cdot C_{1c} - C_1 \cdot C_{3c}}{C_{1c} \cdot m_o \cdot v_T} \tag{5.6-2}$$

For VTS-1, the zero is about a decade below the natural frequency as shown in Figure 5-15 This accentuates peaking in the frequency response. After the resonance frequency, the system falls off at a net of one pole.

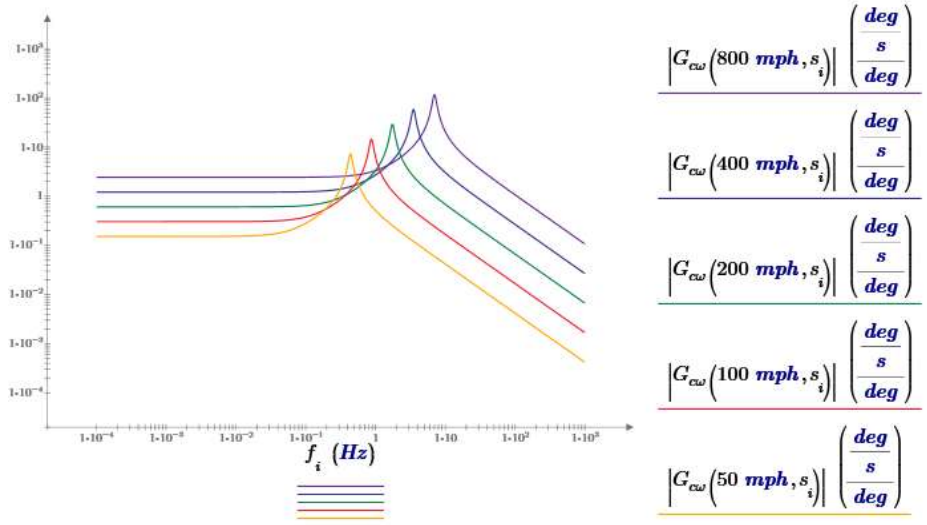

Figure 5-14 Frequency response of the gain from the canard angle to the pitch rotation rate

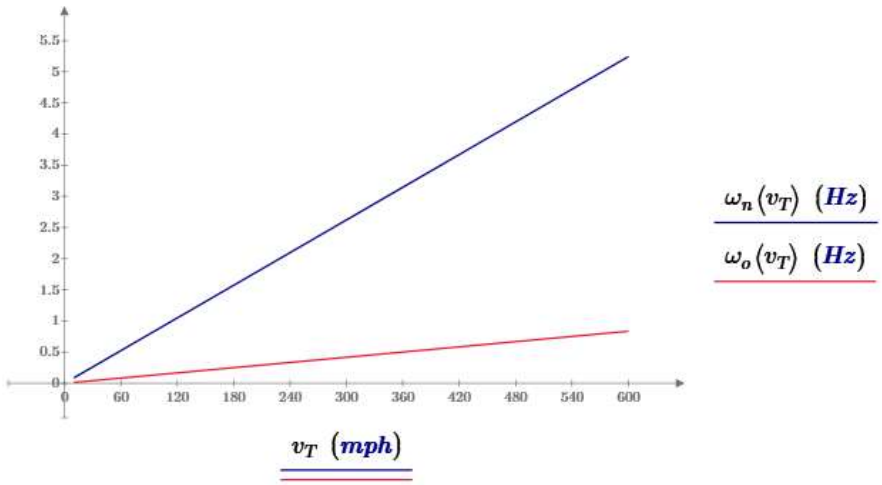

Figure 5-15 Pitch rotation natural frequency, ω_n, and zero frequency, ω_o

Figure 5-16 shows that the steady state pitch rotation rate gain per deg rotation of the canard for VTS-1 from equation (5.6-1) increases linearly with velocity.

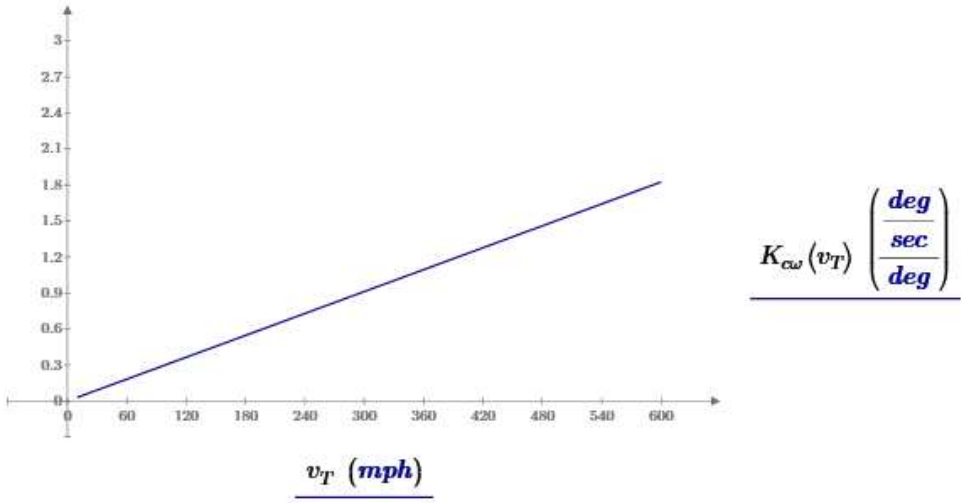

Figure 5-16 Canard pitch rotation gain for VTS-1

To characterize the system in the time domain, a step response is used. In this case, the angle of the canards is stepped, and the pitch rate response is determined. The Laplace transform of a unit step is $1/s$, so the time domain step response is the inverse Laplace transform of equation (5.5-3) times α_c/s, where α_c is the size of the step

$$\mathcal{L}^{-1}\left(\frac{\omega_y}{\alpha_c}\cdot\frac{\alpha_c}{s}\right)=\mathcal{L}^{-1}\left(K_{c\omega}\cdot\frac{\frac{s}{\omega_z}+1}{\left(\frac{s^2}{{\omega_n}^2}+\frac{2\cdot\zeta\cdot s}{\omega_n}+1\right)}\cdot\frac{\alpha_c}{s}\right)= \tag{5.6-3}$$

$$\omega_{out}(t)\Big|_{step}=\alpha_c\cdot K_{c\omega}\cdot\left(\begin{array}{l}\dfrac{{\omega_n}^2-\zeta\cdot{\omega_n}^2\cdot\omega_z}{\omega_z\cdot\sqrt{(-\zeta^2+1)\cdot{\omega_n}^2}}\cdot e^{-(\zeta\cdot\omega_n\cdot t)}\cdot\sin\left(t\cdot\sqrt{(-\zeta^2+1)\cdot{\omega_n}^2}\right)\\ -e^{-(\zeta\cdot\omega_n\cdot t)}\cdot\cos\left(t\cdot\sqrt{(-\zeta^2+1)\cdot{\omega_n}^2}\right)+1\end{array}\right)$$

Figure 5-17 shows a plot of the pitch rotation rate response to a 1 degree step in the canard angle for various airstream velocities. The final value for the step response is the steady state gain, $K_{c\omega}$ times the size of the input step in the canard angle, in this case, 1 degree. A 2 degree step would produce twice the pitch rotation rate shown in the graph.

The amplitude of the overshoot and oscillation is exaggerated by the zero. The flat final response says that, after the initial transient response settles, the rocket rotates in pitch at a constant rate for a given angle rotation of the canards, the same as it does for roll, but a much lower rate.

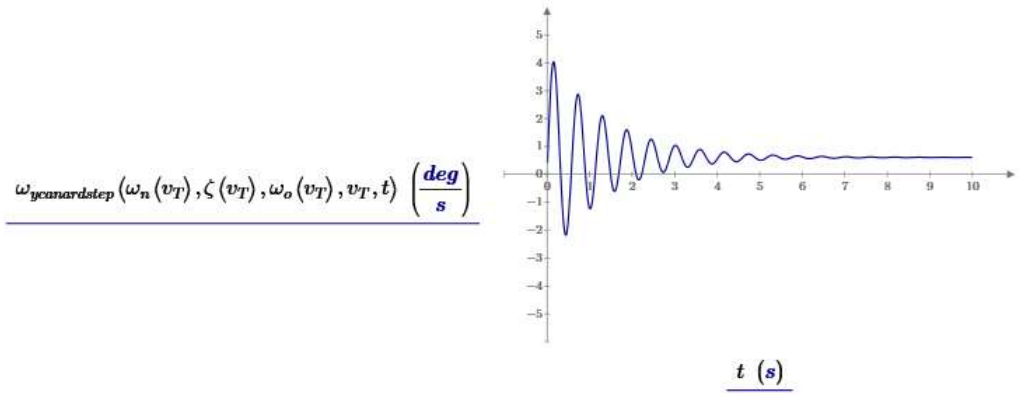

Figure 5-17 Pitch rotation rate response to a step in the canard angle at an airstream velocity of 200 mph

Figure 5-18 shows the Bode plot of magnitude of the transfer function of the canard angle for the pitch rotation angle for various airstream velocities for the vertical orientation test rocket VTS-1 in units of degrees of rotation per degree of canard angle. It is the rotation rate gain multiplied by another integrator. Because of the pole at the origin

due to the output integrator, the system falls off as a single pole at low frequencies. After the resonance frequency, the system falls off at a net of two poles.

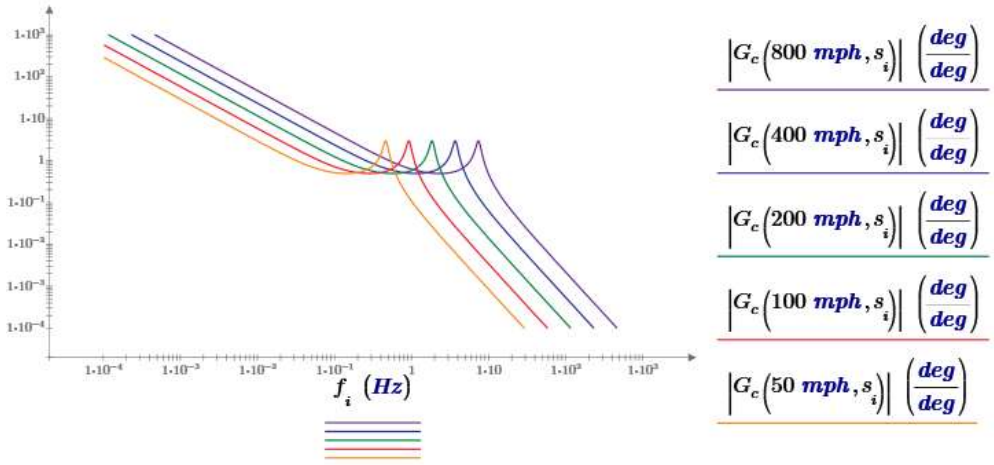

Figure 5-18 Frequency response of the gain from the canard angle to the pitch rotation angle

5.7 Pitch Rate vs Roll Rate Gain due to Canard Angle Rotation

Comparing Figure 4-4 to Figure 5-16, the steady state roll rate gain due to the canard angle is about 1800 times larger than the steady state pitch rate gain for VTS-1. Comparing figures Figure 4-5 and Figure 5-15, the bandwidth of the pitch rotation dynamics is about 7 times larger than the bandwidth of the roll dynamics, so the pitch gain is much lower, but with a larger bandwidth. Figure 5-19 shows the Bode plots for both gains for VTS-1 at an airstream velocity of 200 mph. The difference in gain is not as large above 0.5 Hz due to the difference in bandwidth and second order gain peaking, but there is still a large difference. Why is the roll gain so much larger than the pitch gain for the same rotation of the canards?

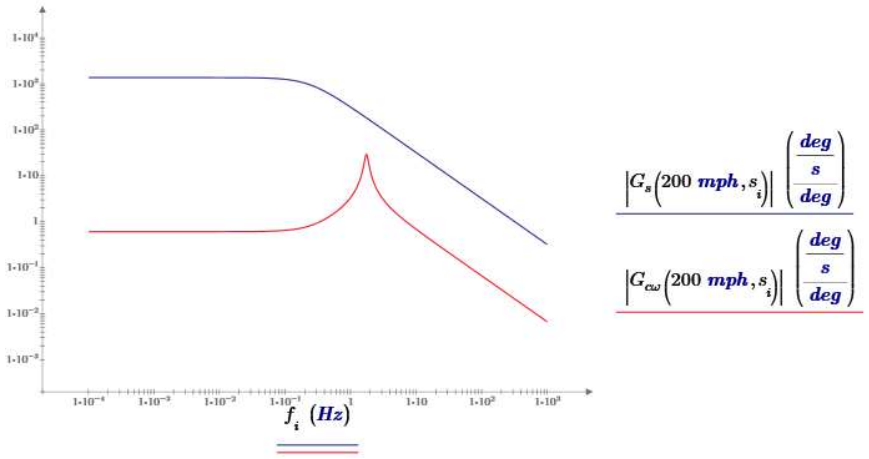

Figure 5-19 Canard roll gain, G_s, and canard pitch gain, $G_{c\omega}$, at $v_T = 200mph$

From equation (4.3-1), the steady state roll rate gain is the ratio of the roll rotation forcing coefficient to the roll damping coefficient, C_{1z}/C_{2z}. The pitch rate gain, from equation (5.6-1) includes coefficients from both the pitch rotation equation and the X-axis equation of motion, due to the coupling between those two equations. If there were no coupling between the two equations, then, from the rotation equation block diagram in Figure 5-3, it can be seen that the pitch rotation rate gain would be the ratio of the pitch forcing coefficient to the pitch damping coefficient, C_1/C_2, much like the roll gain. For VTS-1, the ratio of the roll forcing coefficient to the roll damping coefficient at 200 mph is

$$\left.\frac{C_{1z}}{C_{2z}}\right|_{V_{Tz}=200mph} = 1363 \cdot \frac{\left(\frac{\deg}{s}\right)}{\deg}$$

and the ratio of the pitch forcing coefficient to the pitch damping coefficient is

$$\left.\frac{C_{1c}}{C_2}\right|_{V_{Tz}=200mph} = 251.8 \cdot \frac{\left(\frac{\deg}{s}\right)}{\deg}$$

The ratio of the roll forcing to the roll damping coefficients is 5.4 times the ratio of the pitch forcing to the pitch damping coefficients. The roll rate forcing coefficient is due to all four canards, and the roll damping coefficient is due just to the four canards since the fins provide no damping due to the spin can. The pitch forcing coefficient is due to just two canards, and the damping coefficient is due to two canards and two fins. The number of fins and

canards cancel in the two ratios, but the fins have 6 times the area of the canards, which explains the ratio of the roll rate gain to the ratio of the pitch coefficients. But the actual pitch rotation rate gain is still 333 times the ratio of the pitch forcing to the pitch damping coefficients.

Taking the actual pitch rotation rate gain with the coupled parameters, equation (5.6-1), and rearranging the terms

$$K_{c\omega} = \frac{C_1 \cdot C_{3c} - C_3 \cdot C_{1c}}{C_2 \cdot C_3 + C_1 \cdot m_o \cdot v_T} = \frac{-C_{1c} + \dfrac{C_1 \cdot C_{c3}}{C_3}}{C_2 + \dfrac{C_1 \cdot m_o \cdot v_T}{C_3}} \tag{5.7-1}$$

The coupling adds a term to the forcing coefficient, C_{1c}, in the numerator and a term to the damping coefficient, C_2, in the denominator. Looking at the magnitude of these terms for VTS-1 at 200 mph, in the numerator

$$C_{1c} = -603.0 \cdot \frac{lb \cdot ft^2}{s^2}$$
$$\frac{C_1 \cdot C_{3c}}{C_3} = 221.9 \cdot \frac{lb \cdot ft^2}{s^2}$$

and in the denominator,

$$C_2 = 2.39 \cdot \frac{lb \cdot ft^2}{s}$$
$$\frac{C_1 \cdot m_o \cdot v_T}{C_3} = \left(L_{CP} - L_{CG}\right) \cdot m_o \cdot v_T = 1353 \cdot \frac{lb \cdot ft^2}{s}$$

The coupling term added to the canard forcing coefficient in the numerator is similar in magnitude to the force coefficient, but the term added to the damping coefficient in the denominator is over 500 times the pitch damping coefficient and dominates the magnitude of the denominator and the resulting pitch rate gain. This says that it is the term added by the X-axis equation of motion to the damping coefficient that accounts for most of the reduction in the pitch rotation gain in the coupled system and, other than the portion due to the physical geometry to the rocket fin and canard configuration, is the primary reason for the pitch rotation gain being so much lower than the roll rotation gain,

The author's paper *Rotational Dynamic Stability*[27] showed that the side-to-side motion of the rocket due to the lift force in the X-axis equation of motion caused an induced airstream velocity that added to the tangential rotational velocity, increasing the pitch damping ratio, equation (5.3-7), significantly. This is the damping ratio for the second

[27] (Fetter T. B., Rotational Dynamic Stability - vNARCON 2024 R&D Report, 2024)

order differential equation in the denominator of both the wind transfer function, equation (5.3-1), and canard angle transfer function, equation (5.5-1), so the same enhanced damping seen in the wind transfer function due to the side-to-side motion of the rocket also applies to the canard transfer function. The reduction in gain of the canard transfer function in equation (5.7-1) must also be due to the X-axis motion of the rocket, but more work is needed to understand how the X-axis motion physically causes the canard gain reduction.

It is important to note that the difference in roll and pitch gains is not due to the difference in the longitudinal and lateral moments of inertia (the longitudinal moment of inertia is much larger than the lateral moment of inertia). The bandwidth of the canard roll gain, equation (4.3-2), and canard pitch gain, equation (5.3-6), are functions of the moments of inertia, but the steady state gain, in both cases, is not.

6 Simulation vs. Flight Data Results

The pitch and roll dynamics models presented in this paper were used to design the control system for a vertical orientation rocket. The accuracy of the dynamics models is determined by comparing the flight date from the rocket to the 3-D simulation of rocket's flight as shown in Figure 6-1. The flight simulator is a time domain simulator that includes the aerodynamic rocket model, a dynamic model of the servo motors, and the same control loop functions for pitch, yaw, and roll control that are used in the actual rocket control system. If the models do not match the actual dynamics on the rocket, then the flight simulation will not match the flight data.

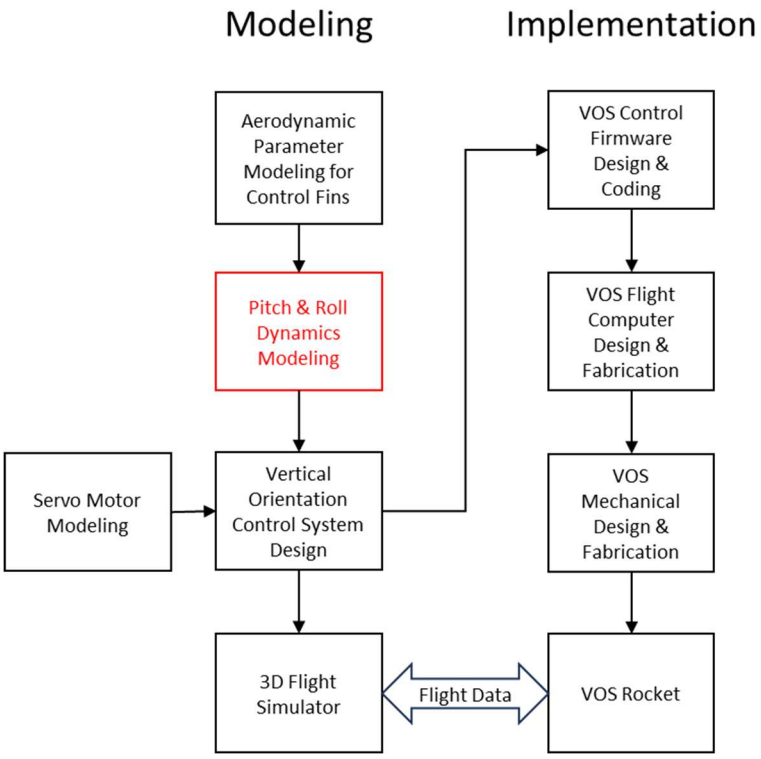

Figure 6-1 Design Process and Model Validation

Figure 6-2 to Figure 6-4 show the simulated and measured flight data for flight 14 of VTS-1 that took place on May 15, 2025, at LDRS, sponsored by TCC in Helm, California. Figure 6-2 shows the roll response. The roll control is a variable gain, optimal state space controller where the poles are held at a fixed optimal location independent of the rocket's velocity by changing the gain as a function of the rocket's velocity. More about the control system design and performance will be covered in the paper on the vertical orientation control system design.

The rocket started out 65 degrees from its absolute target roll angle which was having the positive rocket x-axis pointed due west. The fall time of the simulated response is a little faster than the flight data, and the damping is a little larger, but this is a very close match. In both cases, once the roll reaches the target 0 deg, the controller holds the absolute roll angle at zero without any oscillation due to loop instability. The well controlled response and close match between the simulation and flight data is achievable only if the aerodynamic parameters and rocket rotational dynamics are modeled correctly.

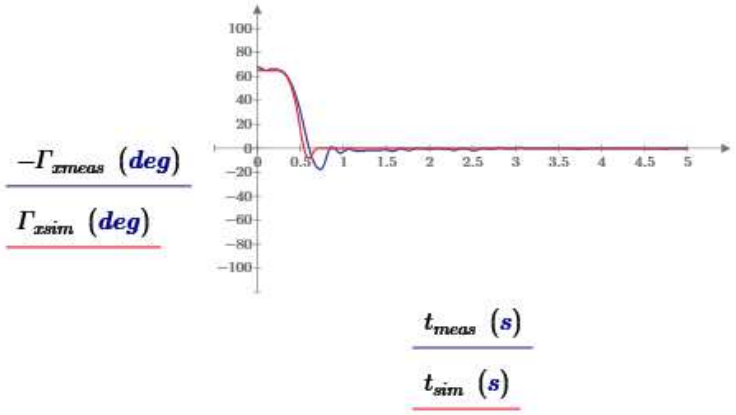

Figure 6-2 Simulated and measured flight data roll response for an initial offset of 65 deg

Figure 6-3 shows the same flight as Figure 6-2, but with the servo motor simulation enabled. The servo motor model includes the servo motor dynamics as well as nonlinear attributes such as quantization and motor hysteresis. The step response shows a larger magnitude oscillation than the simulation without the servo motor. This oscillation caused by the servo motor is due to a limit cycle oscillation rather than the control loop stability dynamics. A limit cycle oscillation is caused by nonlinearities in a control loop. The servo motor model slightly overestimates the effects of the limit cycle oscillation, but it shows that some of the underestimation of the oscillation magnitude in Figure 6-3 is likely due to the servo motor and not a discrepancy in the calculation of the rocket's aerodynamic parameters.

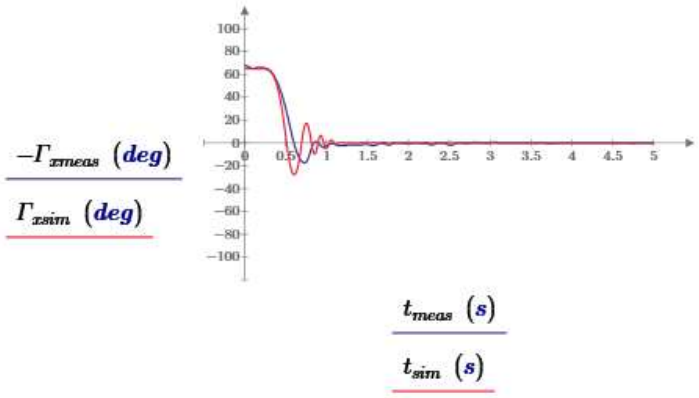

Figure 6-3 Simulated and measured flight data roll response for an initial offset of 65 deg with the servo motor dynamics simulation disabled

Figure 6-4 shows the tilt response. The pitch and yaw control is a fixed gain state space controller where the poles move as a function of the rocket's velocity but are optimized in the center of the rocket's velocity range. Tilt is the polar angle of the rocket's z-axis from vertical and includes the effects of both pitch and yaw rotations. The initial tilt of the launch rail is 2 deg, and the average ground wind speed at launch was ~15 mph. The initial conditions for the wind velocity in the simulation to get a good match with the flight data for the peak rotation is 20 mph. The measured initial rotation of the rocket as the rocket leaves the launch guide occurs earlier than the simulation, but the settling time back to zero is almost identical. The earlier rotation could be due to rail whip which would explain why a larger wind velocity was needed for the simulation. The flight data has about 1 deg of noise most likely due to changes in the wind velocity which is not in the simulation. Overall, this is a very close match. Again, there is no instability in the control loop.

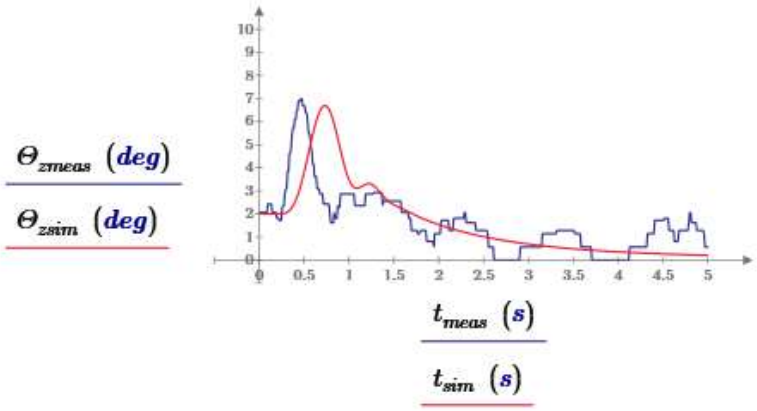

Figure 6-4 Simulated and measured flight data tilt response for an initial launch angle of 2 deg

7 Conclusions, and Next Steps

7.1 Conclusions

The state space block diagrams for yaw/pitch and roll, needed to design and model a vertical orientation control system and rocket flight have been presented. The model parameters are summarized in Appendix 1.

It was shown that the flight data from the vertical orientation test rocket VTS-1 matches the 3-D flight simulator data very closely for both steps in tilt (pitch & yaw) and roll. The vertical orientation control system was designed using the pitch and roll dynamics models for the canards presented in this paper. The control system is implemented in both the 3-D flight model and the VTS-1 flight controller. The well controlled response and close match between the simulation and flight data is achievable only if the aerodynamic parameters and rocket rotational dynamics are modeled correctly.

7.2 Next Steps

- Write the remaining papers to complete the documentation of the vertical orientation control project
- Determine the physical mechanism behind the canard gain reduction due to the coupling between the X-axis equation of motion and the pitch rotation equation

8 Appendix 1 – Model Parameter Summary

Parameter	Value	Source Equation
Pitch Dynamics Block Diagram	See Figure 5-5	
Pitch/Yaw Forcing Coefficient	$C_1 = \frac{\rho}{2} \cdot {v_T}^2 \cdot A_r \cdot \left(L_{CP} - L_{CG}\right) \cdot C_{N\alpha TB}$	(5.1-19)
Pitch/Yaw Canard Forcing Coefficient	$C_{1c} = \frac{\rho}{2} \cdot {v_T}^2 \cdot A_r \cdot \left(L_{CPc} - L_{CG}\right) \cdot C_{N\alpha Tc}$	(5.1-20)
Pitch/Yaw Damping Coefficient	$C_2 = \frac{\rho}{2} \cdot \lvert v_T \rvert \cdot A_r \cdot \left(L_{CP} - L_{CG}\right)^2 \cdot C_{N\alpha}$	(5.1-21)
Forcing Normal Force Coefficient Derivative	$C_{N\alpha TB} = C_{N\alpha nc} + C_{N\alpha Tf} \cdot K_{TBf} + C_{N\alpha Tc} \cdot K_{TBc}$	(5.1-15)
Damping Normal Force Coefficient Derivative	$C_{N\alpha} = C_{N\alpha nc} + C_{N\alpha Tf} + C_{N\alpha Tc}$	(5.1-18)
Rocket Center of Pressure	$L_{CP} = \frac{C_{N\alpha nc} \cdot L_{CPnc} + C_{N\alpha Tf} \cdot K_{TBf} \cdot L_{CPf} + C_{N\alpha Tc} \cdot K_{TBc} \cdot L_{CPc}}{C_{N\alpha nc} + C_{N\alpha Tf} \cdot K_{TBf} + C_{N\alpha Tc} \cdot K_{TBc}}$	(5.1-16)
Pitch/Yaw Lift Coefficient	$C_3 = \frac{\rho}{2} \cdot A_r \cdot C_{L\alpha TB} \cdot {v_T}^2$	(5.1-29)
Pitch/Yaw Canard Lift Coefficient	$C_{3c} = \frac{\rho}{2} \cdot A_r \cdot C_{L\alpha Tc} \cdot {v_T}^2$	(5.1-30)
Lift Force Coefficient Derivative	$C_{L\alpha TB} \simeq C_{N\alpha TB}$	(5.1-31)
Canard Lift Force Coefficient Derivative	$C_{L\alpha Tc} \simeq C_{N\alpha Tc}$	(5.1-32)
Roll Dynamics Block Diagram	See Figure 4-2	
Roll Forcing Coefficient	$C_{1z} = -\frac{\rho}{2} \cdot {v_{Tz}}^2 \cdot A_r \cdot CA_{Rc} \cdot C_{N\alpha Rc}$	(4.1-5)
Roll Damping Coefficient (with spin can)	$C_{2z} = \frac{\rho}{2} \cdot \lvert v_{Tz} \rvert \cdot A_r \cdot {CM_{Rc}}^2 \cdot C_{N\alpha Rc}$	(4.1-6)
Roll Damping Coefficient (without spin can)	$C_{2z} = \frac{\rho}{2} \cdot \lvert v_{Tz} \rvert \cdot A_r \cdot \left({CM_{Rc}}^2 \cdot C_{N\alpha Rc} + {CM_{Rf}}^2 \cdot C_{N\alpha Rf}\right)$	(4.1-7)

See Appendix 1 of *Aerodynamic Parameters for Control Fins*[28] for the fin and canard parameters used in these equations

[28] (Fetter T. B., Aerodynamic Parameters for Control Fins - vNARCON 2026 R&D Report, 2026)

9 Appendix 2 - VTS-1 Test Rocket

VTS-1 is the vertical orientation control rocket, including the custom flight controller, used to gather all the flight data presented in this paper. More information about the VTS-1 project is available on the author's web site[29].

VTS-1 rev4.1
Length: 59.4500 In. , Diameter: 3.1000 In. , Span diameter: 11.1000 In.
Mass 9.116673 Lb. , Selected stage mass 9.116673 Lb.
CG: 35.8127 In., CP: 40.3972 In., Margin: 1.48
Engines: [J350W-0]

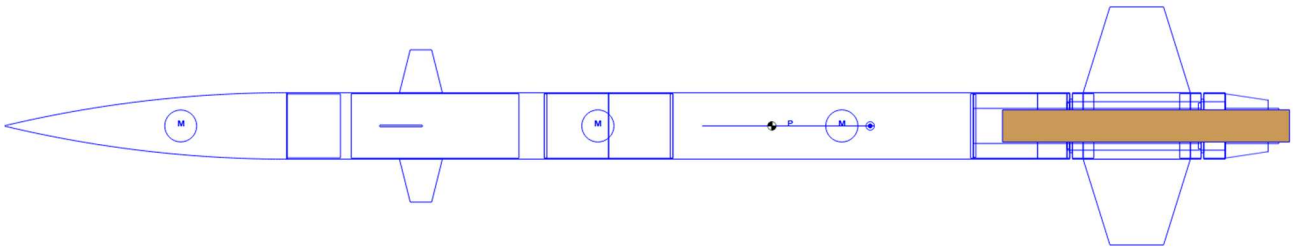

Rocket Diameter	$D_r = 3.124\ in$
Nosecone Length	$L_{nc} = 13.2\ in$
Body tube length	$L_{bt} = 46.25\ in$
Number of fins	$N_f = 4$
Fin root edge length	$c_{rf} = 5\ in$
Fin tip edge length	$c_{tf} = 2.5\ in$
Fin span from body tube	$s_f = 4\ in$
Fin mid cord sweep angle	$\Gamma_{cf} = 0\ deg$
Fin base location	$L_f = 3\ in$
Number of canards	$N_c = 4$
Canard setback length	$L_{sc} = 5\ in$
Canard root edge length	$c_{rc} = 2\ in$
Canard root edge length	$c_{tc} = 1\ in$
Canard span from body tube	$s_c = 2\ in$
Canard mid cord sweep angle	$\Gamma_{cc} = 0$
Mass of the rocket plus motor	$m_o(0 \cdot sec) = 8.955\ lb$
Longitudinal moment of inertia	$I_L = 14.369\ lb \cdot ft^2$
Lateral moment of inertia	$I_R = 0.087\ lb \cdot ft^2$
Center of gravity	$L_{CG_0} = 35.614\ in$
Center of pressure	$L_{CP} = 41.795\ in$

[29] (Fetter T. , 2014-2025)

10 Appendix 3 – State Space Block Diagram of a Differential Equation

A frequency domain differential equation can be represented in the form of a block diagram. If the differential equation is a model of a physical system, then the block diagram provides a visualization of the physical parameters and operation of that system. The block diagram is also a key tool used for designing control systems. The block diagram shows how the control system interfaces to and affects the dynamics of the system being controlled to ensure that the overall system has the desired dynamics and is stable.

The block diagram models the series of simultaneous algebraic polynomials that result from taking the Laplace transform of a series of differential equations. Because the block diagram is based on the Laplace transform of time domain differential equations, it is a frequency domain model of the system[30].

Figure 10-1 shows the block diagram for a simple feedback loop.

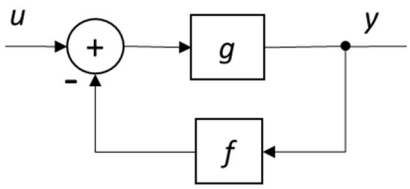

Figure 10-1 Feedback loop

Writing the node equation for the diagram and rearranging it into the form of the gain from the input to the output, results in the transfer function

$$\begin{aligned} y &= u \cdot g - y \cdot g \cdot f \\ \Rightarrow \frac{y}{u} &= \frac{g}{1 + g \cdot f} \end{aligned} \tag{10.1-1}$$

The Laplace transform of an integration operation is $1/s$. In state space block diagrams, a block with the gain of $1/s$ is often represented by the integrator symbol

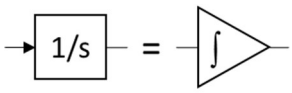

Figure 10-2 Integrator block diagram symbol

[30] See (Friedland, 1986) for a more detailed explanation of state space systems

Figure 10-3 shows a block diagram with an integrator as the gain block in the forward path.

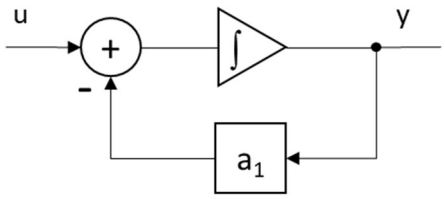

Figure 10-3 First order system

The transfer function for this block diagram using equation (10.1-1) is

$$H(s) = \frac{y}{u} = \frac{1/s}{1 + a_1 \cdot 1/s} = \frac{1}{s + a_1} \tag{10.1-2}$$

The integrator feedback loop topology allows modeling a transfer function where there is a polynomial in terms of the complex frequency parameters in the denominator of the gain function. In this case, the block diagram represents the transfer function for a first order differential equation.

Figure 10-4 shows a two integrator topology where the feedback paths go from the output of the integrators to the summer at the input to the system.

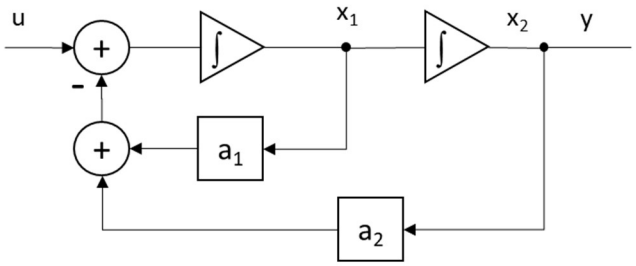

Figure 10-4 Second order system

The transfer function of this second order system is

$$H(s) = \frac{y}{u} = \frac{\frac{1}{s + a_1} \cdot s}{1 + a_2 \cdot \frac{1}{s + a_1} \cdot s} = \frac{1}{s^2 + a_1 \cdot s + a_2} \tag{10.1-3}$$

Figure 10-5 shows how to extend the block diagram to an n[th] order system

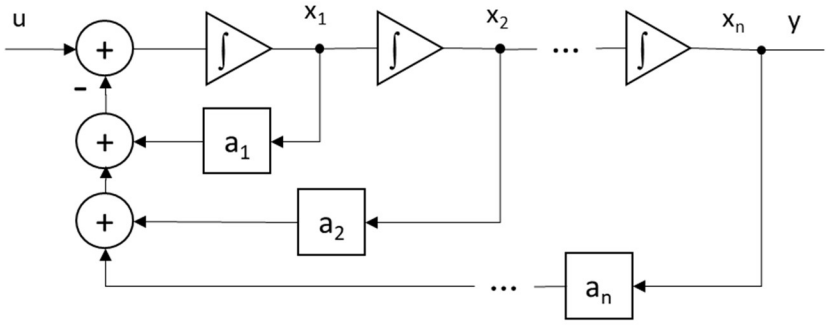

Figure 10-5 n[th] order system

where the transfer function is

$$H(s) = \frac{1}{s^n + a_1 \cdot s^{n-1} + a_2 \cdot s^{n-2} \ldots + a_n} \tag{10.1-4}$$

Summing the feedback at the input of the system conveniently associates each feedback gain with a single coefficient in the corresponding differential equation, so it is very easy to map a differential equation transfer function onto this form of block diagram by inspection. Other block diagram feedback path topologies can also model an n[th] order polynomial, but each coefficient would be comprised of multiple feedback gain values, so the mapping math is more complicated.

Each of the output nodes of the integrators in the block diagram, nodes x_1-x_n in Figure 10-5, represents a state variable of the system. The system has an input, u, and an output, y. State variables are the minimum set of variables needed to describe the complete state of the system. All other parameters of the system can be determined by algebraic equations in terms of the input variable and the state variables. When a set of simultaneous differential equations is represented in terms of first order integrals, it is called the state space representation of the system.

The roots of the polynomial in Equation (10.1-4) are called poles. Poles are the roots in the denominator of the transfer function. The roots of a system that has a polynomial in the numerator are called zeros. A system where

the Laplace transform of the differential equations has a polynomial in the numerator as well as the denominator has a transfer function of the form

$$H(s) = \frac{b_0 \cdot s^m + b_1 \cdot s^{m-1} + b_2 \cdot s^{m-2} \ldots + b_{m-1} \cdot s + b_m}{s^n + a_1 \cdot s^{n-1} + a_2 \cdot s^{n-2} \ldots + a_{n-1} \cdot s + a_n} \tag{10.1-5}$$

and can be modeled by the block diagram topology shown in Figure 10-6. The numerator and denominator polynomials do not need to be of the same order.

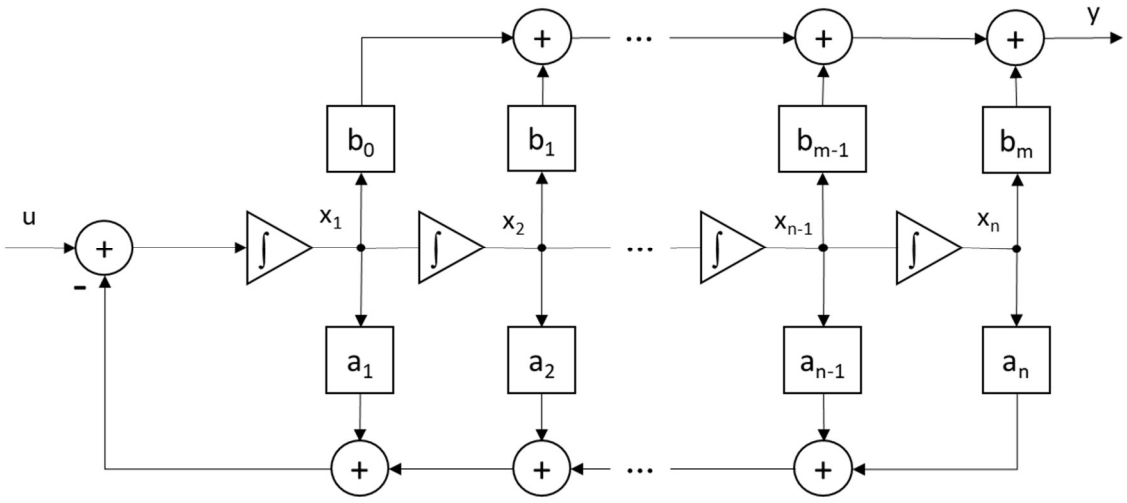

Figure 10-6 General form of state space block diagram for a nth order polynomial in the numerator and denominator

11 Appendix 4 – Pitch Block Diagram Transfer Function Simplification

This section shows the process used to reduce the pitch rotation block diagram block derived in Section 5.2 to a single transfer function for the wind velocity gain and a single transfer function for the canard gain. Since the model is a frequency domain model which was created by taking the Laplace transform of the linear time domain differential equations assuming the airstream velocity, v_T , is a fixed value, the block diagram represents a series of simultaneous linear algebraic equations.

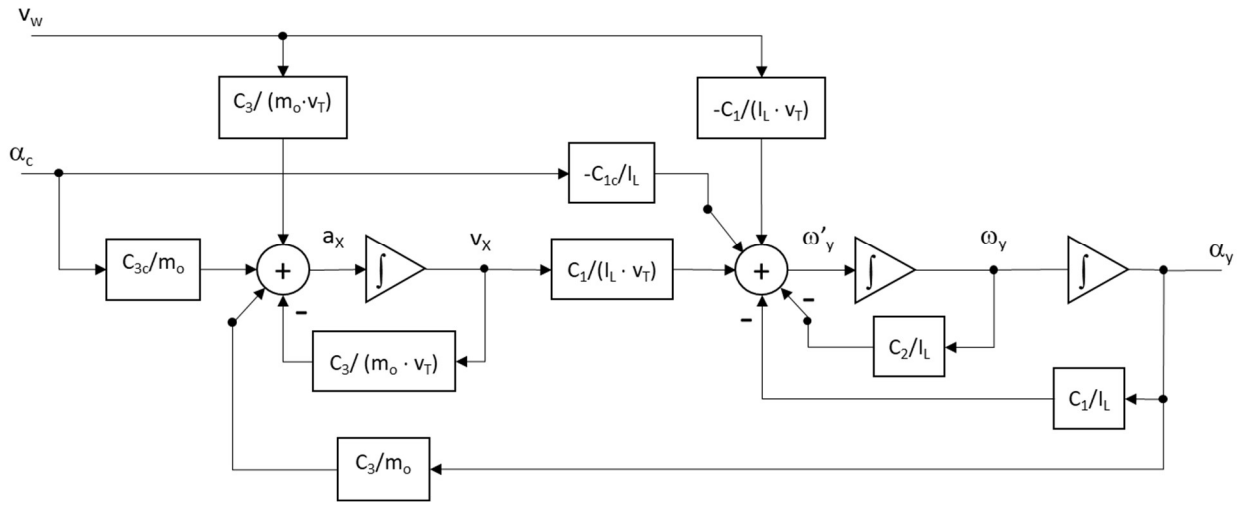

First, the expressions in each of the blocks is replaced by a single representative function to simplify writing the node equations.

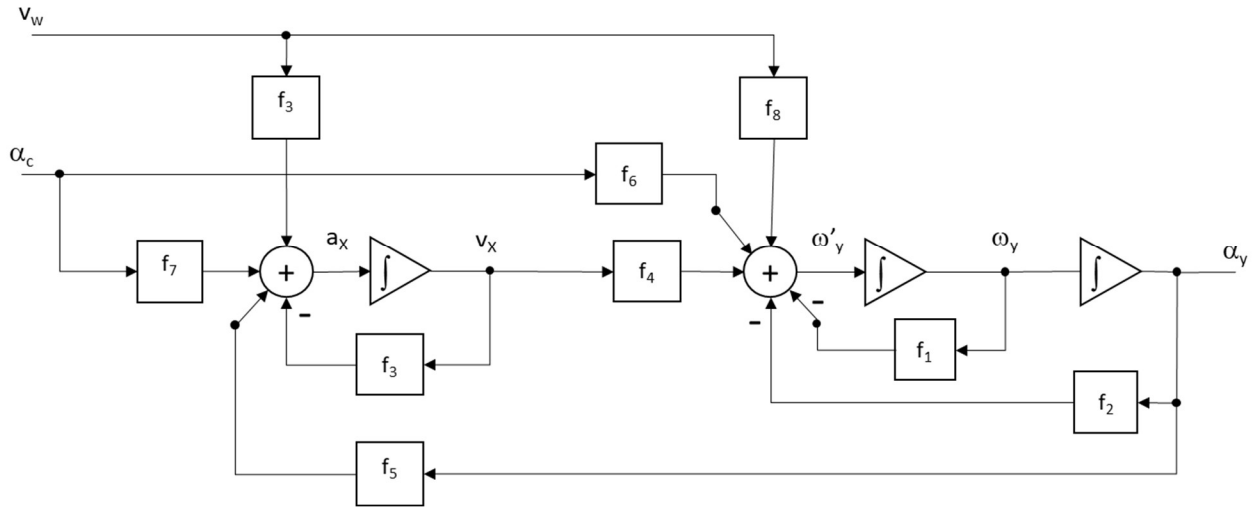

The three integrators, two with their feedback paths, are simplified to single blocks where

$$f_{10} = \frac{1}{s + f_1}$$
$$f_{11} = \frac{1}{s}$$
$$f_{12} = \frac{1}{s + f_3}$$

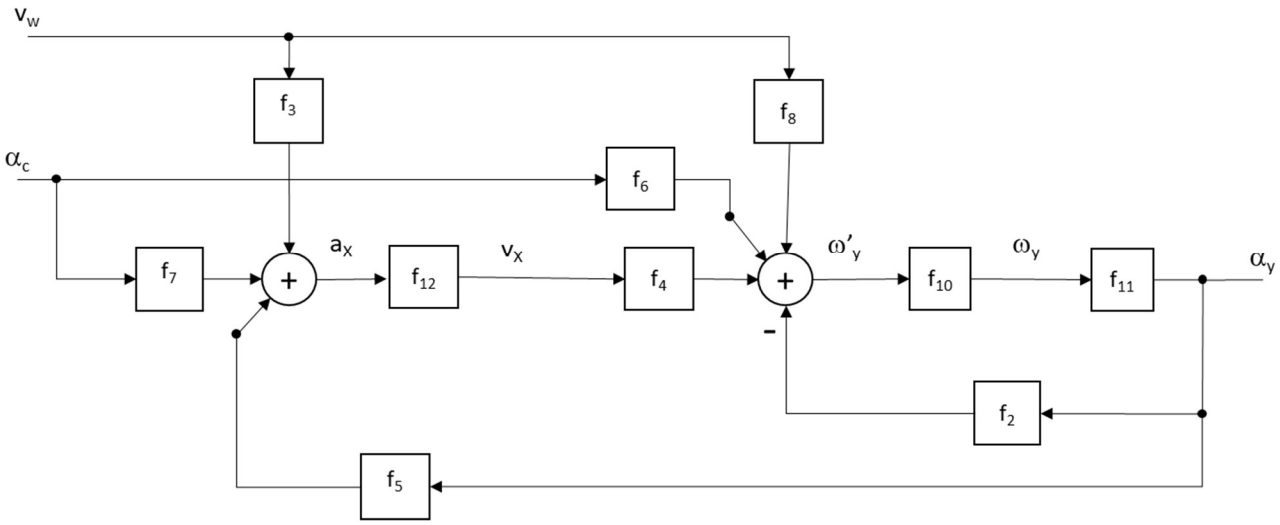

Then the node equations are written. Since there are three state variables, the X-axis velocity, v_X, the y-axis rotation rate, ω_y, and the y-axis rotation angle, α_y, there three simultaneous equations needed to solve for the state variables. The two inputs to the system are the wind velocity, v_w, and the canard rotation angle, α_c. The three node equations are

$$v_X = \alpha_c \cdot f_7 \cdot f_{12} + \alpha_y \cdot f_5 \cdot f_{12} + v_w \cdot f_9 \cdot f_{12}$$
$$\omega_y = \alpha_c \cdot f_6 \cdot f_{10} - \alpha_y \cdot f_2 \cdot f_{10} + v_X \cdot f_4 \cdot f_{10} + v_w \cdot f_8 \cdot f_{10}$$
$$\alpha_y = \omega_y \cdot f_{11}$$

The next figure shows the process used in Mathcad where the three simultaneous linear algebraic equations are first solved for the state variables in terms of the f_x values, then the transfer gain functions are created, and finally the actual parameters are substituted back into the transfer functions.

Simplify the block diagram using terms

$$f_{10} := \frac{1}{s + f_1} \qquad f_{11} := \frac{1}{s} \qquad f_{12} := \frac{1}{s + f_3}$$

Solve the simultaneous algebraic node equations for the State Space form of the Pitch Model

$$\begin{bmatrix} v_X & \omega_y & \alpha_y \end{bmatrix} := \begin{bmatrix} v_X = \alpha_c \cdot f_7 \cdot f_{12} + \alpha_y \cdot f_5 \cdot f_{12} + v_w \cdot f_9 \cdot f_{12} \\ \omega_y = \alpha_c \cdot f_6 \cdot f_{10} - \alpha_y \cdot f_2 \cdot f_{10} + v_X \cdot f_4 \cdot f_{10} + v_w \cdot f_8 \cdot f_{10} \\ \alpha_y = \omega_y \cdot f_{11} \end{bmatrix} \xrightarrow{solve,\, v_X,\, \omega_y,\, \alpha_y} \begin{bmatrix} \left\langle \left(-\left(f_{10} \cdot f_{11} \cdot f_{12} \cdot f_2 \right) \right) \right. \ldots \end{bmatrix}$$

$$v_X \xrightarrow{simplify} \frac{-\left(f_{12} \cdot \left(\left(\left(f_{10} \cdot f_{11} \cdot f_2 + 1 \right) \cdot f_7 + f_{10} \cdot f_{11} \cdot f_5 \cdot f_6 \right) \cdot \alpha_c + \left(\left(f_{10} \cdot f_{11} \cdot f_2 + 1 \right) \cdot f_9 + f_{10} \cdot f_{11} \cdot f_5 \cdot f_8 \right) \cdot v_w \right) \right)}{f_{10} \cdot f_{11} \cdot f_{12} \cdot f_4 \cdot f_5 - \left(f_{10} \cdot f_{11} \cdot f_2 + 1 \right)}$$

$$\omega_y \xrightarrow{simplify} \frac{-\left(f_{10} \cdot \left(\left(f_{12} \cdot f_4 \cdot f_7 + f_6 \right) \cdot \alpha_c + \left(f_{12} \cdot f_4 \cdot f_9 + f_8 \right) \cdot v_w \right) \right)}{f_{10} \cdot f_{11} \cdot f_{12} \cdot f_4 \cdot f_5 - \left(f_{10} \cdot f_{11} \cdot f_2 + 1 \right)}$$

$$\alpha_y \xrightarrow{simplify} \frac{-\left(f_{10} \cdot f_{11} \cdot \left(\left(f_{12} \cdot f_4 \cdot f_7 + f_6 \right) \cdot \alpha_c + \left(f_{12} \cdot f_4 \cdot f_9 + f_8 \right) \cdot v_w \right) \right)}{f_{10} \cdot f_{11} \cdot f_{12} \cdot f_4 \cdot f_5 - \left(f_{10} \cdot f_{11} \cdot f_2 + 1 \right)}$$

Substitute values

$$f_1 := \frac{C_2}{I_L} \qquad f_2 := \frac{C_1}{I_L} \qquad f_3 := \frac{C_3}{m_o \cdot v_T} \qquad f_4 := \frac{C_1}{I_L \cdot v_T}$$

$$f_5 := \frac{C_3}{m_o} \qquad f_6 := \frac{-C_{1c}}{I_L} \qquad f_7 := \frac{C_{3c}}{m_o} \qquad f_8 := \frac{-C_1}{I_L \cdot v_T}$$

$$f_9 := \frac{C_3}{m_o \cdot v_T} \qquad f_{10} := \frac{1}{s + f_1} \qquad f_{11} := \frac{1}{s} \qquad f_{12} := \frac{1}{s + f_3}$$

Create the transfer gain functions

$$G_w := \frac{\alpha_y}{v_w} \xrightarrow{assume,\, \alpha_c = 0} \frac{-\left(f_{10} \cdot f_{11} \cdot f_{12} \cdot f_4 \cdot f_9 + f_{10} \cdot f_{11} \cdot f_8 \right)}{f_{10} \cdot f_{11} \cdot f_{12} \cdot f_4 \cdot f_5 - \left(f_{10} \cdot f_{11} \cdot f_2 + 1 \right)}$$

$$G_c := \frac{\alpha_y}{\alpha_c} \xrightarrow{assume,\, v_w = 0} \frac{-\left(f_{10} \cdot f_{11} \cdot f_{12} \cdot f_4 \cdot f_7 \right) - f_{10} \cdot f_{11} \cdot f_6}{f_{10} \cdot f_{11} \cdot f_{12} \cdot f_4 \cdot f_5 - \left(f_{10} \cdot f_{11} \cdot f_2 + 1 \right)}$$

Reassign the parameters

$$G_w \xrightarrow{simplify} \frac{-\left(C_1 \cdot m_o \right)}{I_L \cdot m_o \cdot v_T \cdot s^2 + \left(C_2 \cdot m_o \cdot v_T + C_3 \cdot I_L \right) \cdot s + C_1 \cdot m_o \cdot v_T + C_2 \cdot C_3}$$

$$G_c \xrightarrow{simplify} \frac{-\left(C_{1c} \cdot m_o \cdot v_T \cdot s \right) + \left(C_1 \cdot C_{3c} - C_{1c} \cdot C_3 \right)}{s \cdot \left(I_L \cdot m_o \cdot v_T \cdot s^2 + \left(C_2 \cdot m_o \cdot v_T + C_3 \cdot I_L \right) \cdot s + C_1 \cdot m_o \cdot v_T + C_2 \cdot C_3 \right)}$$

Rearranging the terms in G_w and G_c to fit the standard state space format results in

$$G_w = \frac{\alpha_y}{v_w} = \frac{-C_1}{I_L \cdot v_T} \cdot \frac{1}{s^2 + \frac{C_2 \cdot m_o \cdot v_T + C_3 \cdot I_L}{I_L \cdot m_o \cdot v_T} \cdot s + \frac{C_2 \cdot C_3 + C_1 \cdot m_o \cdot v_T}{I_L \cdot m_o \cdot v_T}} \tag{11.1-1}$$

$$G_c = \frac{\alpha_y}{\alpha_c} = \frac{-C_{1c}}{I_L} \cdot \frac{s + \frac{C_3 \cdot C_{1c} - C_1 \cdot C_{3c}}{C_{1c} \cdot m_o \cdot v_T}}{s \cdot \left(s^2 + \frac{C_2 \cdot m_o \cdot v_T + C_3 \cdot I_L}{I_L \cdot m_o \cdot v_T} \cdot s + \frac{C_2 \cdot C_3 + C_1 \cdot m_o \cdot v_T}{I_L \cdot m_o \cdot v_T} \right)} \tag{11.1-2}$$

The starting model is a third order system. The canard transfer function is also third order system with a zero. The wind transfer function is a second order system with no zero. This comes about because the paths that would give rise to the higher order system cancel each other out in that transfer function.

12 Appendix 5 - Tools, Equipment, Facilities, & Budget

Software

- Mathcad was the main tool used on this project for modeling, numerical analysis, symbolic analyses, measurement data analysis, and data graphing.
- RockSim was used to validate the parameters calculated by the model such as moment of inertia and center of pressure.
- Microsoft Office Word was used to write this paper
- MathType embedded app for Office was used to create the equations in MS Word
- TurboCAD was used to create most of the figures other than graphs and create the test rocket vertical orientation control system mechanical design

Hardware

- The VTS-1 test rocket was used to validate the pitch and roll aerodynamic parameters

Facilities

- All computer work was done in the author's home office
- Test rocket VTS-1 was built in the author's home woodworking and miscellaneous projects shop including all 3-D printing and control electronics assembly
- All test flights were done at Tripoli Central California's launch site at the Maddox Dairy in Helm California

Project Expenses

	Price	Unit	Used	Cost
VOS Unit				
MD89MW-CAN servo	$ 120.00	1	4	$ 480.00
Servo Hubs	$ 9.69	5	4	$ 7.75
LiPo Battery	$ 23.00	2	1	$ 11.50
SAMD21 Arduino	$ 25.00	1	1	$ 25.00
LSM9DS1 IMU	$ 18.00	1	1	$ 18.00
MPL3115A2 Pressure Sensor	$ 16.75	1	1	$ 16.75
Micro SD Holder	$ 6.00	1	1	$ 6.00
MPC2515 CAN Bus module	$ 10.59	2	1	$ 5.30
AP63357 Buck Regulator	$ 5.95	1	1	$ 5.95
Proto Board	$ 12.29	5	2	$ 4.92
Micro SD card	$ 13.68	2	1	$ 6.84
PLA+	$ 40.00	1	0.5	$ 20.00
Misc hardware	$ 20.00	1	1	$ 20.00
Switch	$ 6.00	1	1	$ 6.00
Total				**$ 634.00**
VTS-1 Rocket				
2" tube	$ 21.29	36	6	$ 3.55
3" tube	$ 25.79	36	42	$ 30.09
1.5" tube	$ 28.04	36	14	$ 10.90
3" Coupler	$ 29.16	36	12	$ 9.72
Fin Stock	$ 42.00	1152	288	$ 10.50
Fiberglass cloth	$ 200.00	31	2	$ 12.90
Shock Cords	$ 1.71	1	30	$ 51.30
Misc Hardware	$ 20.00	1	1	$ 20.00
Motor Retainer	$ 25.00	1	1	$ 25.00
Altus Metrum Easy Mini	$ 80.00	1	2	$ 160.00
Total				**$ 333.96**
Motors				
AT I211W motors	$ 73.00	1	7	$ 511.00
AT J350W or AT420R	$ 96.00	1	8	$ 768.00
e-matches	$ 66.00	80	30	$ 24.75
Total				**$ 1,303.75**
Project Total				**$ 2,271.72**

13 Key Variables

A_r	cross-sectional area of the rocket used to normalize the force coefficients
C_1	pitch forcing coefficient
C_{1z}	roll forcing coefficient
C_2	pitch damping coefficient
C_{2z}	roll damping coefficient
C_3	X-axis lift coefficient
CA_{Rc}	radial center of area of the canards
C_D	drag coefficient
$C_{L\alpha TB}$	lift force coefficient for the complete rocket including the nosecone, canards, and fins, along with the tail/body interference factors for the canards and fins (used for the pitch forcing moment)
$C_{L\alpha Tc}$	lift force coefficient for the canard section not including the tail body interference factor
CM_{Rc}	radius of gyration for the canards
$C_{N\alpha}$	pitch normal force coefficient for the rocket including the nosecone, canards, and fins but not including the tail body interference factors (used for the pitch damping moment)
$C_{N\alpha Rc}$	radial normal force coefficient for the canards
$C_{N\alpha TB}$	pitch normal force coefficient for the complete rocket including the nosecone, canards, and fins, along with the tail/body interference factors for the canards and fins (used for the pitch forcing moment)
$C_{N\alpha Tf}$	pitch normal force coefficient for the fin section not including the tail body interference factor
$C_{N\alpha Tc}$	pitch normal force coefficient for the canard section not including the tail body interference factor
CP	center of pressure
CG	center of gravity
$d_{X,Y,Z}$	distance traveled along the ground frame X,Y,Z-axes
$F_{DX,Y,Z}$	drag force along the ground frame of reference X,Y,Z-axes
$F_{LX,Y,Z}$	the lift force along the ground frame Z,Y,Z-axes
$F_{Nx,y,z}$	the normal force aligned with the rocket frame of reference x,y,z-axes
$F_{TX,Y,Z}$	the thrust force along the ground frame X,Y,Z-axes
g	acceleration due to gravity
I_L	longitudinal moment of inertia
I_R	radial moment of inertia

K_{cp}	dc gain of the canard pitch gain equation
K_s	dc gain of the roll rate gain function
K_{TBc}	pitch body-tail interference factor for the canards due to the angle-of-attack of the body tube
K_{TBf}	pitch body-tail interference factor for the fins due to the angle-of-attack of the body tube
k_{TBc}	pitch body-tail interference factor due to the angle of the canard
K_w	dc gain of the wind pitch gain function
L_{CP}	distance from the tip of the nosecone to the center of pressure
L_{CG}	distance from the tip of the nosecone to the center of gravity
m_o	mass of the rocket
$M_{1x,y,z}$	pitch rotational forcing moment about the rocket frame of reference x,y,z-axes
$M_{2x,y,z}$	pitch rotational damping moment about the rocket frame of reference x,y,z-axes
s	complex frequency $s = j \cdot \omega$
t	time
v_{CG}	the velocity of the center of gravity of the rocket
v_T	the velocity of the total oncoming airstream
v_{Tz}	the rocket frame of reference z-axis component of the total oncoming airstream velocity
v_w	the velocity of the wind along the X-axis
$v_{X,Y,Z}$	the velocity of the rocket along the ground frame X,Y,Z-axes
$v_{x,y,z}$	the velocity of the rocket along the rocket frame x,y,z-axes
x, y, z	axes in the rocket frame of reference
X, Y, Z	axes in the inertial ground-based frame of reference
α_{at}	angle-of-attack between the total oncoming airstream and the z-axis of the rocket body
$\alpha_{cx,y,z}$	rotational angle of the canards aligned with the rocket frame of reference x,y,z-axes
α_T	angle from the Z-axis opposite the direction of the total oncoming airstream
$\alpha_{x,y,z}$	rotational angle about the rocket frame of reference x,y,z-axes
Δ	angle between the direction of travel of the center of gravity of the rocket and the direction the rocket is pointed
Γ	3-D polar coordinate angle of rotation about the Z-axis
ρ	density of air
θ_T	angle from the Z-axis of the angle of the total oncoming airstream

θ_{CG}	angle between the Z-axis and the direction of the movement of the center of gravity of the rocket
Θ	3-D polar coordinate angle from vertical in 3-dimensional space
ϕ, θ, ψ	Euler's angles of rotation
ω_n	natural frequency of the second order pitch gain function
ω_{ns}	corner frequency of the first order roll gain function
$\omega_{x,y,z}$	rate of rotation of the rocket about the rocket frame x,y,z-axes
ζ	damping ratio of a second order system

14 References

Barrowman, J. (1968). *TIR-33 Calculating the Center of Pressure of a Model Rocket.* Centuri Engineering Company.

Fetter, T. (2014-2025). *Speedmotion Rockets*. Retrieved from Speedmotion Rockets: http://speedmotionrockets.com/

Fetter, T. B. (2024). *How Far Does a Rocket Turn Into the Wind.*

Fetter, T. B. (2024). *Linear Systems and Control Systems Overview.* Retrieved from Speedmotion Rockets: http://speedmotionrockets.com/Papers.html

Fetter, T. B. (2024). *Rotational Dynamic Stability - vNARCON 2024 R&D Report.* NAR.

Fetter, T. B. (2026). *Aerodynamic Parameters for Control Fins - vNARCON 2026 R&D Report.* vNARCON R&D Report.

Friedland, B. (1986). *Control System Design - An Introduction to State-Space Methods.* Mineola, New York: Dover Publications, Inc.

Galejs, R. J. (1999, May/June). What Barrowman Left Out. *Sport Rocketry*, pp. 17-19.

LaBudde, E. V. (1999). *A Design Procedure for Maximizing Altitude Performance, NARAM 41.* National Association of Rocketry.

Mandell, G. K., Caporaso, G. J., & Bengen, W. P. (1973). *Topics in Advanced Model Rocketry.* Cambridge: MIT Press.

Sidi, M. J. (2002). *Spacecraft Dynamics & Control.* Cambridge University Press.

Thomson, W. T. (1986). *Introduction to Space Dynamics.* New York: Dover Publications, Inc.